Journal of Geophysical Research, in press, 2000.

Atmospheric sulfur cycle simulated in the global model GOCART: Comparison with field observations and regional budgets

Mian Chin,[1,2] Dennis L. Savoie,[3] Barry J. Huebert,[4] Alan R. Bandy,[5]
Donald C. Thornton,[5] Timothy S. Bates,[6] Patricia K. Quinn,[6]
Eric S. Saltzman,[3,7] and Warren J. De Bruyn[3]

Abstract

We present a detailed evaluation of the atmospheric sulfur cycle simulated in the Georgia Tech/Goddard Global Ozone Chemistry Aerosol Radiation and Transport (GOCART) model. The model simulations of SO_2, sulfate, dimethylsulfide (DMS), and methanesulfonic acid (MSA) are compared with observations from different regions on various timescales. The model agrees within 30% with the regionally averaged sulfate concentrations measured over North America and Europe but overestimates the SO_2 concentrations by more than a factor of 2 there. This suggests that either the emission rates are too high, or an additional loss of SO_2 which does not lead to a significant sulfate production is needed. The average wintertime sulfate concentrations over Europe in the model are nearly a factor of 2 lower than measured values, a discrepancy which may be attributed largely to the sea-salt sulfate collected in the data. The model reproduces the sulfur distributions observed over the oceans in both long-term surface measurements and short-term aircraft campaigns. Regional budget analyses show that sulfate production from SO_2 oxidation is 2 to 3 times more efficient and the lifetimes of SO_2 and sulfate are nearly a factor of 2 longer over the ocean than over the land. This is due to a larger free tropospheric fraction of SO_2 column over the ocean than over the land, hence less loss to the surface. The North Atlantic and northwestern Pacific regions are heavily influenced by anthropogenic activities, with more than 60% of the total SO_2 originating from anthropogenic sources. The average production efficiency of SO_2 from DMS oxidation is estimated at 0.87 to 0.91 in most oceanic regions.

1. Introduction

The Georgia Tech/Goddard Global Ozone Chemistry Aerosol Radiation and Transport (GOCART) model has been used to simulate the atmospheric sulfur cycle. In a companion paper [*Chin et al.*, this issue] we describe the model framework, summarize a 6-year simulation of sulfate and its precursors, and estimate the anthropogenic contributions to the global sulfate burden. Here we compare the model results with field observations in different regions of the world. These comparisons help test the model's ability to capture the spatial and temporal variations of the sulfur species; they also enable us to apply the model to a regional and global analysis of the processes that control the sulfur distributions.

One of the major advantages of using the GOCART model is its fitness to simulate concentrations of atmospheric constituents for any specific time period, thanks to its use of assimilated meteorological data from the Goddard Earth Observing System Data Assimilation System (GEOS DAS). This is particularly important for simulating observations in field campaigns, which are conducted in a relatively short period of time (from several days to several weeks). Since it is a global model that incorporates major atmospheric physical and chemical processes, GOCART can effectively place local observations into a regional and global context.

The focus of this paper is to evaluate model simulations of the atmospheric sulfur cycle. We begin with a brief description of the model (section 2), as details are given in the companion paper [*Chin et al.*, this issue]. We then compare the model results with surface observations over North America and Europe (section 3) as well as over the oceans (section 4). We further compare model-simulated vertical profiles with those measured in several field campaign programs (section 5). The model-calculated budgets for several continental and oceanic regions are also presented (section 6), followed by conclusions (section 7).

2. GOCART Model

The GOCART model is driven by the off-line meteorological data from the GEOS DAS, with a horizontal resolution of 2° latitude by 2.5° longitude and 20-26 vertical layers (vertical resolution depends on the version of GEOS DAS). The GEOS DAS fields are model-assimilated global analyses constrained by meteorological observations, with extensive prognostic and diagnostic fields archived for chemistry transport model applications [*Schubert et al.*, 1993]. Some of the GEOS DAS fields are 6-hour instantaneous values, while others are either 3- or 6-hour averaged quantities. The GEOS DAS data start from January 1980.

The model simulates four sulfur species: SO_2, sulfate, dimethylsulfide (DMS), and methanesulfonic acid (MSA). The following processes are included in sulfur simulations: advection, which is computed by a flux-form semi- Lagrangian method [*Lin and Rood*, 1996]; boundary layer turbulent mixing, which uses a second-order closure scheme [*Helfand and Labraga*, 1988]; moist convection, which is calculated using archived cloud mass flux fields [*Allen et al.*, 1996]; dry deposition, which uses a resistance-in-series algorithm [*Wesely and Hicks*, 1977] as a function of surface type and meteorological conditions; wet deposition, which accounts for the scavenging of soluble species in convective updrafts and rainout/washout in large-scale precipitation [*Balkanski et al.*, 1993]; chemistry, which includes DMS and SO_2 oxidation using prescribed oxidants (OH, NO_3, and H_2O_2 fields from *Müller and Brasseur* [1995]); and emission, which incorporates SO_2 emissions from anthropogenic (72.8 Tg S yr^{-1}), biomass burning (2.3 Tg S yr^{-1}), and volcanic (varies with time) sources, and DMS emission from the oceans (13–16 Tg S yr^{-1}). The anthropogenic emission encompasses SO_2 released from industrial activities, fuel combustion, and transportation [*Olivier et al.*, 1996]. Volcanic emission accounts for SO_2 from both continuously erupting (4.8 Tg S yr^{-1}) [*Andres and Kasgnoc,* 1998] and sporadically erupting (variable) volcanoes [*Simkin and Siebert,* 1994]. DMS emission from the ocean is computed as a product of seawater DMS concentrations [*Kettle et al.*, 1999] and the sea-to-air transfer velocity [*Liss and Merlivat*, 1986] which depends on the sea surface temperature and the surface wind speed. The surface winds used in the model are the remote sensing data from the Special Sensor Microwave Imager (SSM/I) operated on a series of satellites in the Defense Meteorological Satellite Program [*Atlas et al.*, 1996].

The model time step is 20 min for advection, convection, and diffusion, and 60 min for other processes. The model output of sulfur concentrations is saved every 6 hours. In the model-measurements comparisons presented in the next three sections, all the model results are for the time periods when the observations were made.

3. SO_2 and Sulfate in the Polluted Continental Regions

Anthropogenic sulfur emissions are concentrated in the northern hemispheric midlatitudes. To monitor the pollutant concentrations over the source regions, extensive surface monitoring stations have been established in the past few decades, such as the European Monitoring and Evaluation Program (EMEP) in Europe (http://www.nilu.no/projects/ccc/reports.html), and the Eulerian Model Evaluation Field Study (EMEFS), which was conducted under the umbrella of the National Acid Precipitation Program (NAPAP) and included several air quality and precipitation monitoring networks in North America [*McNaughton and Vet,* 1996]. Here we compare model results with measurements taken from 123 EMEFS sites in 1989 and 73 EMEP sites in 1990. Locations of these sites are shown in Figure 1. To evaluate the model's ability to reproduce the observations on both short- and long-term timescales, we present the comparisons in daily and monthly averaged concentrations.

Figure 2 shows the measured and calculated daily concentrations of SO_2 (Figure 2a) and sulfate (Figure 2b) at eight North American (EMEFS) sites. The model captures the large observed day-to-day variations of both SO_2 and sulfate, but overestimates the SO_2 levels and misses the high sulfate episodes in the summer. The seasonal variations at the North American sites are illustrated in Figure 3, which plots the monthly averaged concentrations of SO_2 (Figure 3a) and sulfate (Figure 3b) at sixteen EMEFS sites. SO_2 exhibits a well defined seasonal cycle with a winter maximum and a summer minimum at every location. This seasonal variation is controlled by the SO_2 oxidation rates which are 2 to 4 times faster in the summer than in the winter over the North American region. On the other hand, although there is a winter minimum and a summer maximum of sulfate at most sites, the observed summer maximum is often underestimated by the model, which tends to simulate a peak in August instead of July as seen in most observations at the EMEFS sites. Other observations over the eastern United States [e.g., *Husain and Dutkiewicz,* 1990; *Shaw and Paur,* 1983] also reported a July maximum of sulfate. Furthermore, the model predicts a minimum sulfate concentration in June at the lower-latitude sites of Georgia and Texas, while the observations show only a small valley. This June minimum of sulfate from the model is mainly caused by a strong wet convection over the United States in May and June, especially in the southeastern region. The convective scavenging efficiently removes not only the sulfate from the atmosphere but also its precursor SO_2, thus reducing the sulfate production rates. In comparison, minimum sulfate concentrations in June or July have been observed at four Canadian sites and are reproduced by the model (last row in Figure 3b).

Similar to Figures 2 and 3, the observed daily and monthly SO_2 and sulfate concentrations in 1990 at European sites and the corresponding model results are shown in Figures 4 and 5. The magnitude of the seasonal variation of SO_2 is generally reproduced in the model. This variation is controlled by the seasonal difference in SO_2 oxidation rates, transport patterns, and SO_2 emissions in Europe (highest in winter, lowest in summer [see *Chin et al.*, this issue]). However, model-calculated SO_2 concentrations are typically a factor of 2 too high compared with the observations. An earlier EMEP modeling study also showed an overestimation of SO_2 concentrations in 1989 [*Iversen,* 1993], attributed to an overestimation of SO_2 emission. On the other hand, model-calculated sulfate concentrations and daily variations agree with the observations well within their ranges of standard deviation, except in winter when the simulated sulfate concentrations are much lower than the observed values, especially at higher latitudes. Underestimation of wintertime sulfate over Europe has been reported in several previous model studies with various explanations for the discrepancy [e.g., *Kasibhatla et al.*, 1997; *Koch et al.*, 1999; *Barth et al.*, 2000]. These explanations include too much wet deposition or vertical ventilation, and too little SO_2 oxidation. While all of the above are possible, none of them seems sufficient to account for sometimes a factor of 10 difference between the model and the measurements. The same discrepancy was also reported in the EMEP modeling and measurements comparison studies [*Schaug et al.*, 1993; *Iversen*, 1993], with a systematic low bias in the model at coastal sites. It was suggested that contributions from uncounted sources could be one possible explanation [*Schaug et al.*, 1993].

Here we suggest that a sea-salt component in the data is likely an important source of the discrepancy, as the EMEP sulfate data have not been corrected for sea spray (A.-G. Hjellbrekke, personal communication, 1999). Some observations in Europe reported that the airborne sea-salt concentrations vary from 10 to 100 $\mu g\ m^{-3}$ near the coast and about 3 $\mu g\ m^{-3}$ at a distance of 350 km inland [*Rossknecht et al.*, 1973;

Gustafsson and Franzén, 2000]. If 7–8% of the sea-salt mass is sulfate, based on the typical sodium mass concentrations (0.3) and the sodium/sulfate mass ratio (0.25) in sea-salt, then there could be 0.7–8 μg m^{-3} sea-salt sulfate in the air near the coast and about 0.2 μg m^{-3} inland. The sea-salt contribution is expected to be most significant in winter when sea-salt emissions over the North Atlantic are higher due to strong winds. The precipitation measurements in the EMEP network also indicate that sea-salt sulfate could contribute up to 50–90% in winter at some locations. To test the possible sea-salt contribution to the sulfate aerosol data, we use the preliminary results of the GOCART model simulated monthly averaged sea-salt concentrations below 800 m for 1990 (P. Ginoux, unpublished results, 2000), assuming that 7% of the sea salt mass is sulfate. The modified model results, that is, non-sea-salt sulfate plus sea-salt sulfate, are shown in the dash-dotted lines in Figure 5. This simple modification results in a much better agreement between the modeled and observed sulfate in winter at, for example, High Muffles (United Kingdom), Vanhill (Sweden), and Faeroeme-Akraber (Denmark). It should be noted, however, that what we try to demonstrate here is a possible magnitude rather than a quantitative assessment of the sea-salt sulfate amount in the EMEP data. A quantitative correction will require airborne sea-salt measurements at the EMEP sites.

6 and 7

Figures 6 and 7 summarize an overall comparison of the model results with observations at all EMEFS and EMEP sites in Figure 1, in seasonally and annually averaged quantities. The major discrepancy between the modeled and the observed SO_2 is that the model overestimates the SO_2 levels at a large fraction of these sites, that is, 1/3 of the EMEFS sites and 2/3 of the EMEP sites. On average, the modeled SO_2 concentrations are a factor of 2.4 and 2.7 too high for the EMEFS and EMEP sites, respectively. By contrast, the simulated sulfate concentrations agree with the observations on average to within 30%, despite the overestimation of SO_2. This is because the production of sulfate in the polluted regions is mainly controlled by the H_2O_2 concentrations in cloud, rather than by SO_2. The overestimation of SO_2 and the good simulation of sulfate levels suggest that either the SO_2 emission rates used in the model are too high, or that there is an unaccounted or underestimated loss of SO_2 which does not lead to a significant sulfate production. Such a loss could include an increase of the calculated SO_2 dry deposition rates or, alternatively, an additional deposition of SO_2 on large aerosol particles (such as dust or sea-salt near the coast). On the other hand, the discrepancies between the modeled and observed SO_2 may be partially explained by the location of the measurements. The samplers are usually located close to the surface, often below the shallow inversion layer not resolved in the model, while most SO_2 is released from the smoke stacks above the local inversions. The summertime sulfate deficit over North America in the model (a factor of 1.5 too low on average), caused by the excessive wet scavenging, is clearly revealed in Figure 6. The comparison in Figure 7 demonstrates that when the model results are modified with sea-salt contributions, the winter low bias in the model disappears.

Figure 8

Figure 8 shows the comparisons of annually averaged wet deposition of non-sea-salt sulfate at the EMEFS and EMEP sites. While the model and observations agree within a factor of 2 at a majority of the sites, there are about 6% of the EMEFS sites and 20% of the EMEP sites where the modeled sulfate in precipitation are more than a factor of 2 too low. However, since precipitation intensities and duration vary highly with space and time, the 3-hour and grid area averaged precipitation rates in the model may not be representative of the actual precipitation rates at individual EMEP sites.

4. Sulfate and MSA Over the Oceans

Sulfate and MSA over the oceans have been measured in the University of Miami network over the past 2 decades [e.g., *Savoie and Prospero*, 1989; *Savoie et al.*, 1993]. These measurements have been conducted mainly on islands or at the coast. In addition, long-term sulfate records are also available at the Mauna Loa Observatory in Hawaii [*Huebert et al.*, 2000]. Figure 9 shows the location of the stations. The monthly average values of sulfate and MSA for 16 stations are shown in Figure 10, together with the model results averaged over 6 years of 1989–1994. The sulfate data in Figure 10 are non-sea-salt sulfate; that is, they have been corrected for sea spray.

Figure 9

Figure 1

The first row in Figure 10a compares sulfate at four North Atlantic sites. The model has difficulty reproducing the observed seasonal variations at Barbados and Bermuda, mainly caused by the excessive convective scavenging in May to July: the same problem as seen in the simulation of the EMEFS data in section 3. In contrast, the model-calculated seasonal cycles at the higher latitude sites of Mace Head and Heimaey agree well with the observations. Compar-

isons of sulfate concentrations at four northern Pacific sites are shown in the second row of Figure 10a. These sites are along the transport route of pollutants from East Asia, with Cheju Island located the closest to the continental source and Oahu located the farthest. Sulfate concentrations decrease from Cheju to Oahu, as expected. Both the model and observations show a springtime maximum at Midway and Oahu from the maximum influence of Asian pollutant transport during that season. One interesting feature is the summer minimum in both model and observations at Cheju and Okinawa, contrary to the North Atlantic sites of Barbados and Bermuda where the model shows a summer minimum while the observations do not. This indicates that the wet convection in summer is overestimated in the model at low latitudes near North America, but is probably realistic near Asia.

Sulfate concentrations and seasonal cycles at the Antarctic coast of Mawson and Palmer Station are well simulated by the model (first two plots in the third row of Figure 10a), except in December and January when the model underestimates the sulfate at Mawson and overestimates that at Palmer by nearly a factor of 2. The sulfate levels over the remote oceans reflect the DMS emission rates, which may be too high in December and January near the Palmer Station due to very high seawater DMS concentrations in the model [*Chin et al.*, this issue]. The sulfate levels and temporal variations at other southern hemispheric ocean sites are also reproduced by the model within the range of standard deviation, except at American Samoa where the model underestimates sulfate concentrations by nearly a factor of 4. The model underestimation of both sulfate and MSA (see Figure 10b) at American Samoa is linked to a low DMS emission rate in the tropical Pacifc [*Chin et al.*, this issue, Figure 1].

The last two plots in Figure 10a show the free tropospheric measurements at the high elevation of Izaña (2367 m above sea level) and the Mauna Loa Observatory (3397 m above the sea level). While Mauna Loa receives long-range transport of Asian pollutants in spring, Izana is influenced by the nearby European sources, an influence which is at its maximum in summer due to the convective process. The transport of pollutants to these free tropospheric sites is reproduced by the model, although the concentrations at Mauna Loa in the model are higher than observed values, which may be explained by the fact that the data at Mauna Loa were sorted to eliminate local influences [*Huebert et al.*, 2000].

Figure 10b compares MSA concentrations at the same sites as sulfate in Figure 10a. The only known MSA source is from DMS oxidation by OH, and the major removal process is wet scavenging. As a result, the concentrations and temporal variations of MSA are directly related to DMS emission rates as well as wet scavenging. Similar to the case of sulfate, the modeled summer minimum of MSA at Barbados and Bermuda is caused by the excessive wet scavenging. Modeled MSA concentrations are too low at Cheju Island in late spring and early summer. This is due to the DMS emission being too low rather than the wet scavenging being too high because the modeled sulfate agrees with the observations at the same site where most sulfate is of anthropogenic origin.

Figure 1

Comparisons of the seasonally and annually averaged sulfate and MSA concentrations at all 29 sites in Figure 9 are shown in Figure 11. The model in general agrees with the observations to within a factor of 2 for all seasons with only a few exceptions. Considering the large uncertainties in DMS emission rates and oxidation product yields, it is remarkable that the model reproduces quite well the observed spatial and temporal variations of sulfate and MSA over the oceans. This indicates that the processes of DMS emission, oxidation rates and yields, as well as deposition parameters in the model are climatologically representative of the atmospheric processes.

Figure 1

Unlike the rich database for sulfate and MSA, there are only a few places where long-term DMS and SO_2 records are available, such as Cape Grim [*Ayers et al.*, 1991, 1995] and Amsterdam Island [*Putaud et al.*, 1992]. We plot in Figure 12 the monthly averaged data in 1989 together with the corresponding model results. The model overestimates DMS concentrations in fall and winter for both sites, and produces a minimum in October instead of August as seen in the data. Modeled SO_2 concentrations at Amsterdam Island in summer are higher than the observations, although they overlap with the data within the uncertainty range.

Figure 1

5. SO_2, Sulfate, DMS, and MSA from Field Campaigns

While the fixed station data provide the best records of temporal variations and long-term trends, aircraft measurements are the only means to obtain the vertical distributions of individual species. Here we compare the model results with the aircraft measurements

from the International Global Atmospheric Chemistry (IGAC) coordinated programs of Pacific Exploratory Missions (PEM) and Aerosol Characterization Experiment (ACE). To evaluate the model's capability of capturing the spatial and temporal variations of tracer concentrations on a short timescale, we sample the model results at the closest geographic location and time to the aircraft measurements. The most desirable measurements, however, would be those with a horizontal scale of 200–250 km, which is comparable to the model grid scale.

The NASA PEM-West Phase A (PEM-West A) was conducted in September–October 1991, a period when the Asian outflow was expected to be at a minimum [*Hoell et al.*, 1996], and PEM-West Phase B (PEM-West B) was conducted in February–March 1994, a period when Asian outflow was at the maximum [*Hoell et al.*, 1997]. Another major difference between these two PEM-West experiments is that the free tropospheric SO_2 and sulfate measured in PEM-West A were heavily influenced by the volcanic emissions from Mount Pinatubo, which erupted in June 1991 injecting 20 Mtons of SO_2 into the stratosphere. Hence SO_2 and sulfate over the Pacific Ocean from PEM-West A and PEM-West B have distinct origins and distributions. Figure 13 shows the aircraft flight routes during PEM-West A and B. Comparisons of the modeled DMS, SO_2, and sulfate vertical profiles with the aircraft data are shown in Figure 14. The data used here are 30-min merged quantities in the NASA Global Tropospheric Experiment (GTE) data archive. These data were integrated over a distance of roughly 200 km, which is very similar to the model grid scale.

The seasonal contrast of Asian outflow is clearly illustrated in the top two rows in Figure 14, where both the model and the data show much higher SO_2 and sulfate concentrations in PEM-West B than in PEM-West A, due to a much stronger advection of pollutants in spring than in fall. The Pinatubo influence in SO_2 and sulfate concentrations at high altitudes is evident in the PEM-West A data over the open ocean (third row in Figure 14). This influence is captured by the model, although the modeled sulfate concentrations are about a factor of 2 higher than the data above the marine boundary layer. The discrepancy between the modeled and observed sulfate concentrations above the boundary layer exists for most of the flights in Figure 14. This difference may be partially attributed to the potential loss of aerosol particles in the inlet system used to collect the sulfate [*Huebert et al.*, 1990]. The model does not capture the DMS vertical profiles over the open oceans, a problem which is most likely associated with the model-estimated DMS emission rates.

Another NASA PEM mission, PEM-Tropics A, was conducted during August-September 1996 in the tropical Pacific region, which is relatively free of direct anthropogenic influences [*Hoell et al.*, 1999]. Figure 15 shows the flight routes of two aircraft, a DC-8 and a P-3B, and the model results are compared with the data in Figure 16. As mentioned above, one difficulty in the aircraft measurements of aerosol is the possible loss in the inlet. This loss was minimized in the P-3B measurements since the aerosols were collected with an external sampler that does not suffer from inlet artifacts [*Huebert et al.*, 1990]. The data collected by the two aircraft in their common measurement area near Tahiti and Easter Island are shown in the top two rows in Figure 16. Concentrations of sulfate and MSA recorded by the P-3B are in general higher than those taken by the DC-8, and the model agrees better with the P-3B data. Concentrations near Fiji and New Zealand (DC-8) and Christmas Island (P-3B) are shown in the last two rows in Figure 16. The model overestimates SO_2 concentrations at altitudes above 6 km, but is consistent with the observed DMS profiles.

From October to December 1995 the First Aerosol Characterization Experiment (ACE 1) was conducted in the Southern Ocean south of Australia to study the formation and characterization of marine aerosols in a minimally polluted environment [*Bates et al.*, 1998a]. A majority of the 33 flights was devoted to intensive studies (November 16 to December 13). In addition, there were transect measurements covering a latitudinal range of 76°N to 59°S. Figure 17 shows the flight tracks in the intensive study area. Major sulfur gas and aerosol species in the marine boundary layer, together with several key parameters for calculating DMS emission flux, such as surface wind speed, sea surface temperature, and seawater DMS concentration, were measured on board the National Oceanic and Atmospheric Administration (NOAA) R/V *Discoverer* ship during the ACE 1 intensive period [*Bates et al.*, 1998b; *De Bruyn et al.*, 1998]. The ship track is superimposed in Figure 17 (dotted line). Most samples were from 30-min circular legs, with a diameter of roughly 60 km. This is less than half the dimension of a model grid scale. Aerosols were sampled through the National Center for Atmospheric Research's (NCAR's) Community Aerosol Inlet. Recent measurements have shown that the collection ef-

Figure 1

Figure 1

Figure 1

ficiency of this type of inlet is low for particles larger than 2–3 μm [*Blomquist et al.*, 2000], so these aerosol data are biased by the exclusion of most supermicron non-sea-salt sulfate and MSA. The bias will be more for MSA than for sulfate because of the larger particle size of MSA [*Huebert et al.*, 1993].

We compare the model results with four groups of ACE 1 flight data in Figure 18: The first group includes the data from transect flights from Hawaii to 59°S south of New Zealand, the second group includes data from the flights designed to study new particle production in cumulus clouds outflow, and the last two groups include data from the two Lagrangian experiments A and B. The model reproduces both the concentrations and the vertical distributions for all sulfur species in these four groups, except for MSA which is more than a factor of 2 too high in the model. Possible explanations for the discrepancy of MSA include a high MSA yield from DMS oxidation in the model, or the low bias in the data as mentioned earlier. The model does not capture the relatively high SO_2 concentrations at 5.5 km and misses a few high sulfate values during Lagrangian B.

Figure 19 compares the R/V *Discoverer* shipboard measurements of surface wind speed, sea surface temperature, and seawater DMS concentrations with those used in the model. The surface winds and the sea surface temperatures in the model match very well with the local observations. The monthly averaged seawater DMS concentrations are also close to the in situ measured data except for a few days (e.g., days 332, 333, and 338) when high DMS concentrations (up to 6 nmol L^{-1}) in the seawater were measured. The DMS emission fluxes calculated using the measured parameters versus those using the model input parameters are shown in the last panel of Figure 19.

Modeled atmospheric concentrations of sulfur species are compared with observations on the *Discoverer* in Figure 20. Note that all the model results are at the grid box and time closest to the center of the 3-hour averaged measurement locations and time, while DMS and SO_2 data were taken every 30 min and sulfate and MSA were typically integrated over a 1-day period. Thus the scale of the model is larger than that of the gas measurements but smaller than that of the aerosol measurements. The range of DMS concentrations measured on the ship (30 to more than 300 ppt) is generally reproduced by the model. However, the observed DMS concentrations on days 332 and 333 are much higher than calculated by the model, reflecting an underestimation of the calculated DMS emission. As shown in Figure 19, the measured seawater DMS concentrations on days 332 and 333 are much higher than those from the monthly averaged values used in the model. Both the model and observations show less than 30 ppt of SO_2 and about 50 ppt of sulfate under the typical background conditions (panels 2 and 3 in Figure 20). There were four episodes on days 330, 332, 333, and 343 when the ship encountered air flowing off the Australian continent [*Bates et al.*, 1998b]. During these episodes, elevated SO_2 concentrations were observed reaching up to 1000 ppt [*De Bruyn et al.*, 1998]. These high SO_2 episodes are clearly captured by the model, as shown in Figure 20 (top panel). High concentrations of sulfate during these episodes are also predicted by the model but are missing in the observations. This is partly a result of the relatively long integration sampling time of sulfate on the ship. As reported by *Quinn et al.* [1998], measurements of the aerosol absorption coefficients at higher temporal resolutions responded well with different air mass.

6. Regional Budget

The generally good simulations of sulfur species provide the base for analyzing the regional budgets with the GOCART model. We summarize here the annual budget for several regions where the model results have been evaluated with the observations in the previous sections. These regions include North America (NAM), Europe (EUR), northwestern Pacific (NWP), southwestern Pacific (SWP), tropical eastern Pacific (TEP), and North Atlantic (NAL). We also report the budget of eastern Asia (EAS) here because it is coupled with NWP, even though we have few data in the EAS region. The borders of these seven regions, together with the 1990 annual sulfur emission flux, are shown in Figure 21. Our purpose is to reveal the general features of the regions and compare them with the global budget presented in the companion paper [*Chin et al.*, this issue]. Here all the budgets are based on the 1990 simulation, that is, a normal year before the Pinatubo eruption. Detailed data analysis for individual field campaigns will be presented elsewhere.

6.1. Sulfur Budget in the Polluted Continental Regions

Table 1 shows the column budget of SO_2 and sulfate in the polluted regions of NAM, EUR, and EAS, defined in Figure 21. Anthropogenic emission is the predominant source of SO_2 there, with the highest

emission rate over Europe. However, nearly half of the SO_2 emitted is dry-deposited to the surface. Dry deposition dominates the removal of SO_2 over the continent particularly in winter when SO_2 oxidation is slow. The sulfate production efficiency, which is defined as the amount of sulfate produced relative to the amount of SO_2 emitted, produced, or imported [*Chin et al.*, this issue], is found to be 0.27, 0.24, and 0.33 over the NAM, EUR, and EAS regions, respectively. These values indicate that only 1/4–1/3 of the SO_2 emitted is oxidized to sulfate within the region, the rest being either removed by deposition or transported out of the region. In-cloud oxidation of SO_2 accounts for roughly 2/3 of the total sulfate production across the three regions, a value which is comparable to the global mean of 64% [*Chin et al.*, this issue]. Both SO_2 and sulfate are much more efficiently removed within the polluted column than outside the column because most of the burden is at lower altitudes near the sources (Table 1). This can be seen in the loss frequency, which is the quantity of the loss rate in the individual process divided by the column burden [*Chin et al.*, this issue]. For example, the loss frequency for SO_2 dry deposition is 0.47–0.53 day^{-1} and for sulfate wet scavenging is 0.24–0.36 day^{-1} in the polluted regions, while the corresponding global mean values are 0.25 and 0.16 day^{-1}, respectively [*Chin et al.*, this issue]. The lifetime is 1.1–1.4 days for SO_2 and 2.8–3.6 days for sulfate in these regions.

If the difference between the total source and total sink is used to infer the net outflow to the neighboring regions, then about 16%, 23%, and 11% of the anthropogenically emitted SO_x (SO_2 plus sulfate) are transported out of the NAM, EUR, and EAS regions, with 2/3 of it as SO_2 (Table 1). The export flux is much lower than that estimated for eastern North America in previous studies ranging from 30% to 59% [*Wojcik and Chang*, 1997; and references therein]. The major difference is that the dry deposition loss for SO_2 in this study is much higher (50%) than that in the previous estimates (17–36%). However, as we have discussed in section 3, the model results of SO_2 over the polluted regions suggest that a higher SO_2 loss rate is required. The net export for the EUR region is 23%, which is within the wide range of previous estimates in the literature (8–80% [see *Wojcik and Chang*, 1997]).

6.2. Sulfur Budget in the Oceanic Regions

Table 2 is the column sulfur budget over the four oceanic regions defined in Figure 21. The NAL region receives a significant amount of anthropogenic SO_2 from the neighboring continents, that is, about 40% of the total SO_2 source. This influx may be overestimated, if the modeled SO_2 concentrations are in fact an overestimate (section 3). Ship emissions account for another 24% of the anthropogenic SO_2 source in the NAL. *Capaldo et al.* [1999] estimated that 40–80% of the surface SO_2 over the North Atlantic region in July is from ship emission. We have examined the July surface SO_2 budget of the NAL region and estimate that 65% of the SO_2 source in the model surface layer (0–50 m) is from ship emission. However, the large contributions of ship emission to SO_2 concentrations are likely limited to near the surface; we have found that in the lowest 2-km column, DMS oxidation is a factor of 1.75 higher than ship emission as the SO_2 source over NAL in July. Therefore it appears in our model that both the continental outflow and DMS oxidation (36%) are more important than ship emission as the SO_2 and sulfate source over the North Atlantic region. Similar to NAL, the anthropogenic input from continents is the largest source of SO_2 in the NWP region (56%). Ship emissions contribute only 5% of the SO_2 source. Accordingly, the total anthropogenic source of SO_2 over the NWP region is 61%, similar to the fraction of 64% over the NAL. The remaining 39% of SO_2 is from DMS oxidation (32%) and volcanic emission (7%).

Unlike the polluted regions of NAL and NWP, Table 2 shows that only 12% of the SO_2 source in the SWP region is from outside of the column. While DMS oxidation is the most important SO_2 source (53%), volcanic emission is also significant; it contributes more than 30% of the SO_2 source in the SWP region. The TEP is the cleanest region among the four with little direct anthropogenic emission. With only 7% of SO_2 from volcanic emissions and 16% imported, DMS oxidation accounts for 77% of the regional SO_2 source.

The annually averaged emission rate of DMS is quite similar at about 90–100 $\mu g\ S\ m^{-2}\ d^{-1}$ among the NWP, SWP, and TEP, but is much higher in the NAL at 190 $\mu g\ m^{-2}\ d^{-1}$, mainly because of the higher surface wind speeds. The most important loss process for SO_2 over the oceans is in-cloud oxidation, in contrast to the continental regions where dry deposition dominates the SO_2 loss. One exception is in the NAL region where dry deposition is as important an SO_2 sink as in-cloud oxidation because the SO_2 is more concentrated near the surface due to its source from ship emissions.

Our model estimates that globally 90% of DMS is oxidized by OH (to produce SO_2 and MSA) and 10% by NO_3 (to produce SO_2) [*Chin et al.*, this issue]. However, the DMS+NO_3 reaction pathway can become more important in places influenced by anthropogenic activities. As seen in Table 2, DMS oxidation by NO_3 accounts for 26% of the total DMS loss over NAL and 12% over NWP, compared with that in the relatively clean regions of SWP (5%) and TEP (2%). The SO_2 production efficiency from DMS (the amount of SO_2 produced relative to the amount of DMS emitted) is 0.91, 0.90, 0.87, and 0.90 for the NAL, NWP, SWP, and TEP regions, respectively. These values are at the high end of those estimated from a zero-dimensional (0-D) photochemical model, i.e., 0.65 to 0.9, for altitudes below 2 km at the tropical Pacific and southern oceans [*Davis et al.*, 1999; *Chen et al.*, 2000; *Shon et al.*, 2000]. Constrained by the measured DMS and SO_2 concentrations, the 0-D model has to assume other parameters, such as the vertical mixing rate and SO_2 lifetime, in order to estimate the SO_2 production efficiency. The lifetime of SO_2 below 2 km is assumed to be 1 day in the 0-D model with respect to the chemical losses, the depositions, and the vertical dilution. The SO_2 production efficiency would be higher if a shorter lifetime were used. For example, our model estimates 0.5–0.7 days for SO_2 lifetime in the marine boundary layer with respect to chemical losses and depositions. A much lower value of SO_2 production efficiency was suggested by *Yvon and Saltzman* [1996] and *De Bruyn et al.* [1998] (0.3–0.5), based on a box model and measured DMS and SO_2 concentrations at the surface. However, vertical mixing was neglected in these studies. One can underestimate the SO_2 production efficiency if vertical mixing is not considered, since vertical mixing is an important transport mechanism for SO_2 from the boundary layer, where most SO_2 is produced, to the free troposphere. As seen in sections 4 and 5, our model results are consistent with the observations over the oceans not only in the marine boundary layer, but also in the free troposphere.

Sulfate production from SO_2 is much more efficient over the oceans than over the polluted continents. Its production efficiency is 0.53, 0.55, 0.55, and 0.66 for the NAL, NWP, SWP, and TEP regions, respectively, compared with 0.24–0.34 over the polluted regions. This is because the fraction of column SO_2 in the free troposphere is larger over the oceans than over the land, hence less loss to surface. Consequently, the lifetimes of SO_2 and sulfate over the oceans are nearly a factor of 2 longer. The contrast of SO_2 vertical distributions between the continental and oceanic regions can be seen in Tables 1 and 2. While 2/3 to 3/4 of the SO_2 over the continents resides below 2 km, a similar fraction is above 2 km over the oceans.

Several recent studies have shown that oxidation on sea-salt surface is an important pathway for SO_2 loss. For example, *Sievering et al.* [1999] estimated from ACE 1 measurements that SO_2 oxidation in sea-salt aerosols could account for 30–35% of the non-sea-salt sulfate formation, and *Mari et al.* [1999] found that sea-salt losses contributed to 37–63% of total SO_2 loss during the Lagrangian B experiment in ACE 1. We have not explicitly included the SO_2 losses in sea-salt aerosols in our model, but found reasonable agreement with the observed SO_2 and sulfate data shown in sections 4 and 5. Long-term ocean surface measurements of SO_2, together with sulfate, are needed to test the magnitude of model error in omission of SO_2 loss in sea-salt. It is possible, however, that the modeled SO_2 in-cloud oxidation and/or dry deposition rates are sufficiently higher than those in the real world that they could be counted as total SO_2 heterogeneous oxidation and total deposition.

7. Conclusions

We have presented a detailed evaluation of the atmospheric sulfur cycle simulated in the GOCART model. We have compared the simulated SO_2, sulfate, DMS, and MSA concentrations with the observations over polluted continental source regions, anthropogenically modified oceans, and in remote environments. The comparisons have been conducted on various time scales from multiyear surface networks to short-term aircraft campaigns. The model in general reproduces the observed spatial and temporal distributions and captures the local and regional features.

Over the polluted regions of North America and Europe where the sources are thought to be well understood, the model reproduces the seasonal variations of SO_2 but overestimates the atmospheric level of SO_2 by more than a factor of 2 on average. On the other hand, the modeled sulfate levels agree with the observations within 30% as the sulfate production rates are controlled by the oxidant concentrations. The model results suggest that either the SO_2 emission rates are too high or an increased SO_2 loss which does not lead to significant sulfate production is required. Such a loss could include an increase of the calculated SO_2 dry deposition rate over the land,

or an additional deposition of SO_2 on large aerosol particles. In the summer season over North America the calculated sulfate levels are 1.5 to 2 times too low compared with observations. This is caused by efficient wet scavenging during summer in the model, which removes not only sulfate, but also its precursor SO_2, thus reducing sulfate production rates. The common difficulty among most models in reproducing the sulfate seasonal variations over Europe may be attributed largely to the sea-salt component in the EMEP data. The sea-salt contribution is expected to be largest in the winter because of high sea-salt emission rates from the neighboring North Atlantic Ocean. When the model results are modified to reflect the sea-salt contribution, the low winter bias in the model disappears. It should be noted, however, that other possible sources could also contribute to the model's low bias in winter, such as a slow SO_2 oxidation rate or strong vertical ventilation in winter.

The modeled sulfur concentrations over the global oceans are consistent with the observations. The multiyear model simulation agrees with the sulfate and MSA climatology not only for the averaged concentrations, but also for the seasonal variations. On the other hand, the model also reproduces the observed DMS, SO_2, sulfate, and MSA concentrations from several field campaigns on a timescale from several hours to a few days on mobile platforms. The model captures the observed large contrast of SO_2 and sulfate vertical profiles between the PEM-West A and PEM-West B, which reflects the seasonal difference in Asian outflow and the influence of volcanic eruptions. The model also reproduces the observations during PEM-Tropics A and ACE 1 in the marine environments that are relatively free of anthropogenic pollution. Overall, our simulations are consistent with the observations in both the marine boundary layer and the free troposphere.

We have estimated that about 16%, 23%, and 11% of the anthropogenically emitted sulfur in North America, Europe, and eastern Asia are transported out to the neighboring oceans. This anthropogenic outflow has a large impact on the sulfur budget over the oceans, especially in the North Atlantic and northwestern Pacific regions. Our budget calculations indicate that about 60% of total SO_2 over these two regions is of anthropogenic origin. Ship emission is estimated to contribute 65% of SO_2 at the surface of the North Atlantic; but the impact of ship emissions is concentrated mostly near the surface. Within the atmospheric column over the North Atlantic, DMS oxidation is 50% more important than ship emissions as the SO_2 source. In contrast to the polluted North Atlantic and northwestern Pacific, the predominant SO_2 source in the southwestern and tropical eastern Pacific is from DMS oxidation. We have estimated that the production efficiency of SO_2 from DMS oxidation is 0.87 to 0.91 in most oceanic regions. These values are higher than those estimated in some 0-D model studies, a discrepancy which is likely due to the transport or loss parameters assumed in the 0-D models.

The sulfate production efficiency from SO_2 oxidation is much lower over the polluted continents than over the oceans. With about half of the SO_2 emitted over the land being deposited to the surface, only 24% to 33% of them are oxidized to produce sulfate over the land. By contrast, 53% to 66% of the SO_2 over the oceans converts to sulfate in the atmosphere. This is because of a larger free tropospheric fraction of column SO_2 over the oceans than over the land, hence less surface loss. The lifetimes of SO_2 and sulfate over the oceans are nearly twice as long as those over the land.

The model-simulated sulfur concentrations are generally in agreement with the observations under a variety of conditions and on different spatialscales and timescales. However, the parameters used in the model, such as wet scavenging, DMS emission, and chemical mechanisms, are highly simplified mainly due to the lack of better knowledge or resource, and some potentially important pathways, such as SO_2 loss in sea-salt aerosols, are not included in the current model. Therefore large uncertainties still exist in quantifying each process involved in the atmospheric sulfur cycle. Nonetheless, the detailed evaluation of the GOCART model provides a solid base for investigating the processes that control the sulfur distributions in the atmosphere, analyzing the relationship that exists between the sulfate aerosol and its precursors, and estimating the forcing that sulfate aerosol exerts on global climate.

Acknowledgments. We thank Doug Davis of Georgia Tech for very helpful discussions, Paul Ginoux of Georgia Tech/GSFC for calculating sea-salt concentrations, Gao Chen of Georgia Tech for providing merged ACE 1 data, Anne M. Thompson of GSFC for commenting on this manuscript, Anne-Gunn Hjellbrekke of the Norwegian Institute for Air Research for providing the EMEP data, and Frank McGovern for helpful discussions of the EMEP data. Comments from two anonymous reviewers are gratefully acknowledged. The EMEFS data were collected and

prepared under the cosponsorship of the United States Environmental Protection Agency, the Atmospheric Environment Service, Canada, the Ontario Ministry of Environment, the Electric Power Research Institute, and the Florida Electric Power Coordinating Group. This research is sponsored by the NASA Atmospheric Chemistry Modeling and Analysis Program, Global Aerosol Climatology Program, EOS/Interdisciplinary Science Program, Goddard Space Flight Center, and NOAA Aerosol Program.

References

Allen, D. J., P. Kasibhatla, A. M. Thompson, R. B. Rood, B. G. Doddridge, K. E. Pickering, R. D. Hudson, and S.-J. Lin, Transport-induced interannual variability of carbon monoxide determined using a chemistry and transport model, *J. Geophys. Res., 101,* 28,655-28,669, 1996.

Andres, R. J., and A. D. Kasgnoc, A time-averaged inventory of subaerial volcanic sulfur emissions, *J. Geophys. Res., 103,* 25,251-25,261, 1998.

Atlas, R., R. N. Hoffman, S. C. Bloom, J. C. Jusem, and J. Ardizzone, A multiyear global surface wind velocity dataset using SSM/I wind observations, *Bull. Am. Meteorol. Soc., 77,* 869-882, 1996.

Ayers, G. P., J. P. Ivey, and R. W. Gillett, Coherence between seasonal cycles of dimethyl sulphide, methanesulphonate and sulphate in marine air, *Nature, 349,* 404-406, 1991.

Ayers, G. P., S. T. Bentley, J. P. Ivey, and B. W. Forgan, Dimethylsulfide in marine air at Cape Grim, 41°S, *J. Geophys. Res., 100*, 21,013-21,021,1995.

Balkanski, Y.J., D.J. Jacob, G.M. Gardner, W.C. Graustein, and K.K. Turekian, Transport and residence times of tropospheric aerosols inferred from a global three-dimensional simulation of ^{210}Pb, *J. Geophys. Res., 98,* 20,573-20,586, 1993.

Barth, M., P. J. Rasch, J. T. Kiehl, C. M. Benkovitz, and S. E. Schwartz, Sulfur chemistry in the National Center for Atmospheric Research Community Climate Model: Description, evaluation, features, and sensitivity to aqueous chemistry, *J. Geophys. Res., 105,* 1387-1415, 2000.

Bates, T. S., B. J. Huebert, J. L. Gras, F. B. Griffiths, and P. A. Durkee, International Global Atmospheric Chemistry (IGAC) Project's First Aerosol Characterization Experiment (ACE 1): Overview, *J. Geophys. Res., 103,* 16,297-16,318, 1998a.

Bates, T. S., V. N. Kapustin, P. K. Quinn, D. S. Covert, D. J. Coffman, C. Mari, P. A. Durkee, W. J. De Bruyn, and E. S. Saltzman, Processes controlling the distribution of aerosol particles in the lower marine boundary layer during the First Aerosol Characterization Experiment (ACE 1), *J. Geophys. Res., 103,* 16,369-16,384, 1998b.

Blomquist, B. W., B. J. Huebert, S. G. Howell, M. Litchy, C. Twohy, D. Baumgardner, B. Lafleur, R. Seebaugh, and M. Laucks, An evaluation of the Community Aerosol Inlet for the NCAR C-130, submitted to *J. Atmos. Oceanic Technol.*, in press, 2000.

Capaldo, K., J. J. Corbett, P. Kasibhatla, P. Fischbeck, and S. N. Pandis, Effects of ship emissions on sulphur cycling and radiative climate forcing over the ocean, *Nature, 400,* 743-746, 1999.

Chen, G., D. D. Davis, P. Kasibhatla, A. R. Bandy, D. C. Thornton, B. J. Huebert, A. D. Clarke, and B. Blomquist, A study of DMS oxidation in the tropics: Comparison of Christmas Island field observations of DMS, SO_2, and DMSO with model simulations, *J. Atmos. Chem., 37,* 137-160, 2000.

Chin, M., R. B. Rood, D. J. Allen, M. O. Andreae, A. M. Thompson, S.-J. Lin, R. M. Atlas, and J. V. Ardizzone, Processes controlling dimethyl sulfide over the ocean: Case studies using a 3-D model driven by assimilated meteorological fields, *J. Geophys. Res., 103,* 8341-8353, 1998.

Chin, M., R. B. Rood, S.-J. Lin, J.-F. Müller, and A. M. Thompson, Atmospheric sulfur cycle simulated in the global model GOCART: Model description and global properties, *J. Geophys. Res.*, this issue.

Davis, D. D., et al., Dimethyl sulfide oxidation in the equatorial Pacific: Comparison of model simulations with field observations for DMS, SO_2, H_2SO_4(g), MSA(g), MS, and NSS, *J. Geophys. Res., 104,* 5765-5784, 1999.

De Bruyn, W. J., T. S. Bates, J. M. Cainey, and E. S. Saltzman, Shipboard measurements of dimethyl sulfide and SO_2 southwest of Tasmania during the First Aerosol Characterization Experiment (ACE 1), *J. Geophys. Res., 103,* 16,703-16,712, 1998.

Gustafsson, M. E. R., and L. G. Franzén, Inland transport of marine aerosols in southern Sweden, *Atmos. Environ., 34,* 313-325, 2000.

Helfand, H. M., and J. C. Labraga, Design of a nonsingular level 2.5 second-order closure model for the prediction of atmospheric turbulence, *J. Atmos. Sci., 45,* 113-132, 1988.

Hoell, J. M., D. D. Davis, S. C. Liu, R. Newell, M. Shipham, H. Akimoto, R. J. McNeal, R. J. Bendura, and J. W. Drewry, Pacific Exploratory Mission-West A (PEM-West A): September-October 1991, *J. Geophys. Res., 101,* 1641-1653, 1996.

Hoell, J. M., D. D. Davis, S. C. Liu, R. E. Newell, H. Akimoto, R. J. McNeal, and R. J. Bendura, Pacific Exploratory Mission-West B (PEM-West B): February-March 1994, *J. Geophys. Res., 102,* 28,223-28,239, 1997.

Hoell, J. M., D. D. Davis, D. J. Jacob, M. O. Rodgers, R. E. Newell, H. E. Fueberg, R. J. McNeal, J. L. Raper, and R. J. Bendura, Pacific Exploratory Mission in the tropical Pacific: PEM-Tropics A, August-September 1996, *J. Geophys. Res., 104,* 5567-5583, 1999.

Huebert, B. J., G. Lee, and W. L. Warren, Airborne

aerosol inlet passing efficiency measurement, *J. Geophys. Res., 95,* 16,369-16,381, 1990.

Huebert, B. J., S. Howell, P. Laj, J. E. Johnson, T. S. Bates, P. K. Quinn, V. Yegorov, A. D. Clarke, and J. N. Porter, Observations of the atmospheric sulfur cycle on SAGA-3, *J. Geophys. Res., 98,* 16,985-16,995, 1993.

Huebert, B. J., C. A. Phillips, L. Zhuang, E. Kjellstrom, H. Rodhe, and J. Feichter, Long-term measurements of free-tropospheric sulfate at Mauna Loa: Comparison with model simulations, *J. Geophys. Res.*, in press, 2000.

Husain, L., and V. A. Dutkiewicz, A long-term (1975-1988) study of atmospheric SO_4^{2-}: Regional contributions and concentration trends, *Atmos. Environ., Part A, 24,* 1175-1187, 1990.

Iversen, T., Modelled and measured transboundary acidifying pollution in Europe - Verification and trends, *Atmos. Environ., Part A, 27,* 889-920, 1993.

Kasibhatla, P., W. L. Chameides, and J. St. John, A three-dimensional global model investigation of seasonal variations in the atmospheric burden of anthropogenic sulfate aerosols, *J. Geophys. Res., 102,* 3737-3759, 1997.

Kettle, A. J., et al., A global database of sea surface dimethylsulfide (DMS) measurements and a simple model to predict sea surface DMS as a function of latitude, longitude, and month, *Global Biogeochem. Cycles, 13,* 399-444, 1999.

Koch, D., D. Jacob, I. Tegen, D. Rind, and M. Chin, Tropospheric sulfur simulation and sulfate direct radiative forcing in the GISS GCM, *J. Geophys. Res., 104,* 23,799-23,823, 1999.

Lin, S.-J., and R. B. Rood, Multidimensional flux-form semi-Lagrangian transport schemes, *Mon. Weather Rev., 124,* 2046-2070, 1996.

Liss, P. S., and L. Merlivat, Air-sea gas exchange rates: Introduction and synthesis, in *The Role of Air-Sea Exchange in Geochemical Cycling,* edited by P. Buat-Ménard, D. Riedel, pp. 113-127, Norwell, Mass., 1986.

Mari, C., K. Suhre, R. Rosset, R. S. Bates, B. J. Huebert, A. R. Bandy, D. C. Thornton, and S. Businger, One-dimensional modeling of sulfur species during the First Aerosol Characterization Experiment (ACE 1) Lagrangian B, *J. Geophys. Res., 104,* 21,733-21,750, 1999.

McNaughton, D. J., and R. J. Vet, Eulerian Model Evaluation Field Study (EMEFS): A summary of surface network measurements and data quality, *Atmos. Environ., 30,* 227-238, 1996.

Müller, J.-F., and G. Brasseur, A three-dimensional chemical transport model of the global troposphere, *J. Geophys. Res., 100,* 16,445-16,490, 1995.

Olivier, J. G. J., A. F. Bouwman, C. W. M. Van der Maas, J. J. M. Berdowski, C. Veldt, J. P. J. Bloss, A. J. H. Vesschedijk, P. Y. J. Zandveld, and J. L. Haverlag, Description of EDGAR Version 2.0: A set of global emission inventories of greenhouse gases and ozone-depleting substances for all anthropogenic and most natural sources on a per country basis and on $1^\circ \times 1^\circ$ grid, *RIVM/TNO Rep. 771060 002,* Rijkinstituut voor Volksgezondheid en Milieu, Bilthoven, Netherlands, Dec. 1996.

Putaud, J. P., N. Mihalopoulos, B. C. Nguyen, J. M. Campin, and S. Belviso, Seasonal variations of atmospheric sulfur dioxide and dimethylsulfide concentrations at Amsterdam Island in the southern Indian Ocean, *J. Atmos. Chem., 15,* 117-131, 1992.

Quinn, P. K., D. J. Coffman, V. N. Kapustin, T. S. Bates, and D. S. Covert, Aerosol optical properties in the marine boundary layer during the First Aerosol Characterization Experiment (ACE 1) and the underlying chemical and physical aerosol properties, *J. Geophys. Res., 103,* 16,547-16,564, 1998.

Rossknecht, G. F., W. P. Eliot, and F. L. Ramsey, The size distribution and inland penetration of sea-salt particles, *J. Appl. Meteorol., 12,* 825-830, 1973.

Savoie, D. L., and J. M. Prospero, Comparison of oceanic and continental sources of non-sea-salt sulphate over the Pacific Ocean, *Nature, 339,* 685-687, 1989.

Savoie, D. L., J. M. Prospero, R. J. Larsen, F. Huang, M. Izaguirre, T. Huang, T. H. Snowdon, L. Custals, and C. G. Sanderson, Nitrogen and sulfur species in Antarctic aerosols at Mawson, Palmer Station, and Marsh (King George Island), *J. Atmos. Chem., 17,* 95-122, 1993.

Schaug, J., R. Iversen, and U. Pedersen, Comparison of measurements and model results for airborne sulphur and nitrogen components with kriging, *Atmos. Environ., Part A, 27,* 831-844, 1993.

Schubert, S. D., R. B. Rood, and J. Pfaendtner, An assimilated data set for earth science applications, *Bull. Am. Meteorol. Soc., 74,* 2331-2342, 1993.

Simkin, T., and L. Siebert, *Volcanoes of the World,* 2nd ed., Geosci., Tucson, Ariz., 1994.

Shaw, R. W., and R. J. Paur, Measurements of sulfur in gases and particles during sixteen months in the Ohio River Valley, *Atmos. Environ., 17,* 1431-1438, 1983.

Shon, Z.-H., et al., Evaluation of the DMS flux and its conversion to SO_2 over the southern ocean, *Atmos. Environ.,* in press, 2000.

Sievering, H., B. Lerner, J. Slavich, J. Anderson, M. Posfai, and J. Cainey, O_3 oxidation of SO_2 in sea-salt aerosol water: Size distribution of non-sea-salt sulfate during the First Aerosol Characterization Experiment (ACE 1), *J. Geophys. Res., 104,* 21,707-21,718, 1999.

Thornton, D. C., A. R. Bandy, B. W. Blomquist, A. R. Driedger, and T. P. Wade, Sulfur dioxide distribution over the Pacific Ocean 1991-1996, *J. Geophys. Res., 104,* 5845-5854, 1999.

Wesely, M. L., and B. B. Hicks, Some factors that affect the deposition rates of sulfur dioxide and similar gases on vegetation, *J. Air Pollut. Control Assoc., 27,* 1110-1116, 1977.

Wojcik, G. S., and J. S. Chang, A re-evaluation of sulfur budgets, lifetimes, and scavenging ratios for eastern North America, *J. Atmos. Chem., 26*, 109-145, 1997.

Yvon, S. A., and E. S. Saltzman, The sulfur dioxide budget in the tropical South Pacific marine boundary layer (12°S, 135°W), *J. Geophys. Res., 101*, 6911-6918, 1996.

A. R. Bandy and D. C. Thornton, Department of Chemistry, Drexel University, Philadelphia, PA 19104. (bandyar @drexel.edu; dct@drexel.edu)

T. S. Bates and P. K. Quinn, Pacific Marine Environmental Laboratory, NOAA, Seattle, WA 98115. (bates@pmel.noaa.gov; quinn@pmel.noaa.gov)

M. Chin, NASA Goddard Space Flight Center, Code 916, Greenbelt, MD 20771. (chin@rondo.gsfc.nasa.gov)

W. J. De Bruyn and D. L. Savoie, Rosenstiel School of Marine and Atmospheric Sciences, University of Miami, Miami, FL 33149. (dsavoie@rsmas.miami.edu; debruyn@rsmas.miami.edu)

B. J. Huebert, Department of Oceanography, University of Hawaii, Honolulu, HI 96822. (huebert@soest.hawaii.edu)

E. S. Saltzman, National Science Foundation, Arlington, VA 22230 (esaltzma@nsf.gov)

Received March 23, 2000; revised June 15, 2000; accepted June 16, 2000.

[1]School of Earth and Atmospheric Sciences, Georgia Institute of Technology, Atlanta.

[2]NASA Goddard Space Flight Center, Greenbelt, Maryland.

[3]Rosenstiel School of Marine and Atmospheric Sciences, University of Miami, Miami, Florida.

[4]Department of Oceanography, University of Hawaii, Honolulu.

[5]Department of Chemistry, Drexel University, Philadelphia, Pennsylvania.

[6]Pacific Marine Environmental Laboratory, NOAA, Seattle, Washington.

[7]Now at National Science Foundation, Arlington, Virginia.

This preprint was prepared with AGU's LaTeX macros v5.01. File s2 formatted August 21, 2000.

Figure 1. Locations of the North American sites in the EMEFS network and European sites in the EMEP network.

Figure 2a. Daily concentrations of SO_2 in 1989 at eight North American sites. Vertical grey lines are observations, and continuous black lines are the model results.

Figure 2b. Same as Figure 2a, but for sulfate.

Figure 3a. Monthly averaged concentrations of SO_2 in 1989 at 16 North American sites. Solid circles are observations, and thick continuous lines are the model results. Standard deviation of daily values are plotted in vertical lines for observations and shaded grey area for the model.

Figure 3b. Same as Figure 3a, but for sulfate.

Figure 4a. Daily concentrations of SO_2 in 1990 at eight European sites. Vertical grey lines are observations, and continuous black lines are model results.

Figure 4b. Same as Figure 4a, but for sulfate.

Figure 5a. Monthly averaged concentrations of SO_2 in 1990 at 16 European sites. Solid circles are observations, and thick continuous lines are the model results. Standard deviation of daily values are plotted in vertical lines for observations and shaded grey area for the model.

Figure 5b. Same as Figure 5a, but for sulfate. The dash-dotted lines are the model results modified to reflect sea-salt contributions. See text for details.

Figure 6. Comparison of seasonally and annually averaged (left) SO_2 and (right) sulfate concentrations in 1989 at 123 North American sites. Site locations are shown in Figure 1. Solid line indicates a perfect match of the model results with observations, and dotted lines denote a factor of 2 departure. Correlation coefficients are indicated in the parenthesis.

Figure 7. Comparison of seasonally and annually averaged (left) SO_2 and (middle and right) sulfate concentrations in 1990 at 73 European sites. Site locations are shown in Figure 1. Solid line indicates a perfect match of the model results with observations, and dotted lines denote a factor of 2 departure. Correlation coefficients are indicated in the parenthesis. The model results in the middle column are non-sea-salt sulfate concentrations, while those in the right column are modified to reflect sea-salt contributions. See text for details.

Figure 8. Comparison of annually averaged sulfate in precipitation at (left) the EMEFS sites for 1989 and (right) the EMEP sites for 1990.

Figure 9. Locations of the oceanic sites in the University of Miami network and the Mauna Loa Observatory.

Figure 10a. Monthly averaged concentrations of sulfate at 16 oceanic sites. Solid circles are observations, and thick continuous lines are the model results. Standard deviation of daily values are plotted in vertical lines for observations and shaded grey area for the model. The data are multiyear averages (number of years varies with sites), and the model results are 6-year averages from 1989 to 1994.

Figure 10b. Same as Figure 10a, but for MSA (no MSA data at Mauna Loa).

Figure 11. Comparison of seasonally and annually averaged (left) sulfate and (right) MSA concentrations at 29 oceanic sites. Sites locations are shown in Figure 9. Solid line indicates a perfect match of the model results with observations, and dotted lines denote a factor of 2 departure. Correlation coefficients are indicated in the parenthesis.

Figure 12. Monthly averaged concentrations of DMS at Cape Grim and DMS and SO_2 at Amsterdam Island for 1989. Solid circles are observations, and lines are the model results. Shaded areas are the standard deviation of daily values in the model.

Figure 13. DC-8 aircraft flight tracks in (left) PEM-West A (September–October 1991) and (right) PEM-West B (February–March 1994). Solid circles are the locations of the following: A, Anchorage; G, Gram; H, Hawaii; J, Japan; K, Hong Kong; N, NASA Ames. Flight numbers are shown next to the tracks.

Figure 14. Vertical profiles of SO_2, sulfate, and DMS from the DC-8 aircraft during PEM-West A (PWA) and PEM-West B (PWB). Grey circles are observations, and crosses are the model results. Flight numbers in each data group are shown in parenthesis.

Figure 15. Aircraft flight tracks in PEM-Tropics A (August–September 1996) for (left) DC-8 and (right) P-3B. Solid circles are the locations of the following: C, Christmas Island; E, Easter Island; F, Fiji; G, Guayaquil; H, Hawaii; N, NASA Ames; T, Tahiti; Z, New Zealand. Flight numbers are shown next to the tracks.

Figure 16. Vertical profiles of SO_2, sulfate, DMS, and MSA from the DC-8 and P-3B aircraft during PEM-Tropics A. Grey circles are observations, and crosses are the model results. Flight numbers in each data group are shown in parenthesis.

Figure 17. C-130 aircraft flight tracks (solid thin lines) in ACE 1 intensive (November–December 1995) study area. Flight numbers are shown next to the tracks. The R/V *Discoverer* ship tracks are shown in thick grey dotted line.

Figure 18. Vertical profiles of SO_2, sulfate, DMS, and MSA from the C-130 aircraft during ACE 1. Each row represents a group of data (see text). Grey circles are observations, and crosses are the model results. Flight numbers in each data group are shown in parenthesis.

Figure 19. Input parameters used for calculating DMS emission rates during ACE 1 intensive period (November–December 1995). Measured (top) surface winds, (second from top) sea surface temperatures, and (third from top) seawater DMS concentrations are shown in solid dots, and those used in the model are shown in continuous lines. The bottom panel is the DMS emission rates calculated from the parameters measured on the R/V *Discoverer* (solid dots) and those used in the model (line).

Figure 20. Time series of DMS, SO_2, sulfate, and MSA from the R/V *Discoverer* during ACE 1 intensive period (November–December 1995). Observations are shown in either solid dots (for DMS and SO_2) or horizontal bars (for sulfate and MSA). The lengths of the horizontal bars correspond to the data integration time. The continuous lines are the model results.

Figure 21. Borders of three continental and four oceanic regions in the budget analysis. NAM, North America; EUR, Europe; EAS, eastern Asia; NAL, North Atlantic; NWP, northwestern Pacific; SWP, southwestern Pacific; and TEP, tropical eastern Pacific.

Table 1. Sulfur Budgets of 1990 for Three Polluted Continental Regions

Regional Budget[a]	NAM	EUR	EAS
SO_2			
Emission	2280	4600	3130
Chemical production	35	56	25
In-air oxidation	222	416	341
In-cloud oxidation	411	684	707
Dry deposition	1110	2610	1490
Wet scavenging	250	145	347
Inferred export[b]	322	801	270
Column burden	2090	5490	3370
Burden below 2 km	1410	4100	2340
Lifetime[c]	1.1	1.4	1.2
Sulfate			
Emission	70	238	157
In-air production	222	416	341
In-cloud production	411	684	707
Dry deposition	81	165	132
Wet scavenging	558	859	977
Inferred export[b]	64	309	96
Column burden	1040	3780	2910
Burden below 2 km	798	1860	1380
Lifetime[c]	3.4	3.6	2.8
Total sulfur			
Dry deposition (percent of source)	49.9%	56.8%	49.0%
Wet scavenging (percent of source)	33.9%	20.5%	40.0%
Inferred export (percent of source)	16.2%	22.7%	11.0%

[a]NAM, North America, surface area 1.49×10^{13} m^2; EUR, Europe, surface area 1.49×10^{13} m^2; EAS, eastern Asia, surface area 1.44×10^{13} m^2. Borders of each region are shown in Figure 21. Units: flux, μg S m^{-2} d^{-1}; burden, μg S m^{-2}; lifetime, days.

[b]Inferred from the difference between the total source and the total loss terms within the column.

[c]Defined as the ratio of column burden to the total loss rate excluding transport.

Table 2. Sulfur Budgets of 1990 for Four Oceanic Regions

Regional Budget[a]	NAL	NWP	SWP	TEP
SO_2				
Anthropogenic emission[b]	92	13	15	0.4
Volcanic emission	0	18	37	8.5
Chemical production	141	87	75	87
Inferred import[c]	152	149	17	20
In-air oxidation	73	57	15	26
In-cloud oxidation	130	91	64	50
Dry deposition	135	71	36	18
Wet scavenging	48	47	29	21
Column burden	919	658	211	275
Burden below 2 km	288	197	81	57
Lifetime[d]	2.8	2.4	1.6	2.4
Sulfate				
Anthropogenic emission[b]	2.9	0.6	0.8	0
In-air production	73	57	15	26
In-cloud production	130	91	64	50
Inferred import[c]	58	56	10	21
Dry deposition	21	13	5.4	8.6
Wet scavenging	243	192	85	88
Column burden	1740	1150	536	749
Burden below 2 km	542	322	119	211
Lifetime[d]	6.6	5.8	6.2	7.8
DMS				
Emission	185	107	91	96
Oxidation by OH	115	85	81	94
Oxidation by NO_3	40	12	4.1	1.9
Inferred export[c]	30	10	5.7	0.1
Column burden	136	92	210	102
Burden below 2 km	114	63	160	80
Lifetime[d]	0.88	0.95	2.7	1.1
MSA				
Chemical production	13.6	10.1	11.0	9.7
Dry deposition	1.1	0.5	0.8	0.8
Wet scavenging	10.3	8.8	10	8.7
Column burden	54	43	62	61
Burden below 2 km	15	7.5	17	13
Lifetime[d]	5.3	4.6	6.1	6.3

[a]NAL, North Atlantic, surface area 2.36×10^{13} m^2; NWP, northwestern Pacific, surface area 2.73×10^{13} m^2; SWP, southwestern Pacific, surface area 2.00×10^{13} m^2; TEP, tropical eastern Pacific, surface area 6.05×10^{13} m^2. Borders of each region are shown in Figure 21. Units: Flux, μg S m^{-2} d^{-1}; burden, μg S m^{-2}; lifetime, days.

[b]Including ship, aircraft, and industrial emissions over the islands.

[c]Inferred from the difference between the total source and the total loss terms within the column.

[d]Defined as the ratio of column burden to the total loss rate excluding transport.

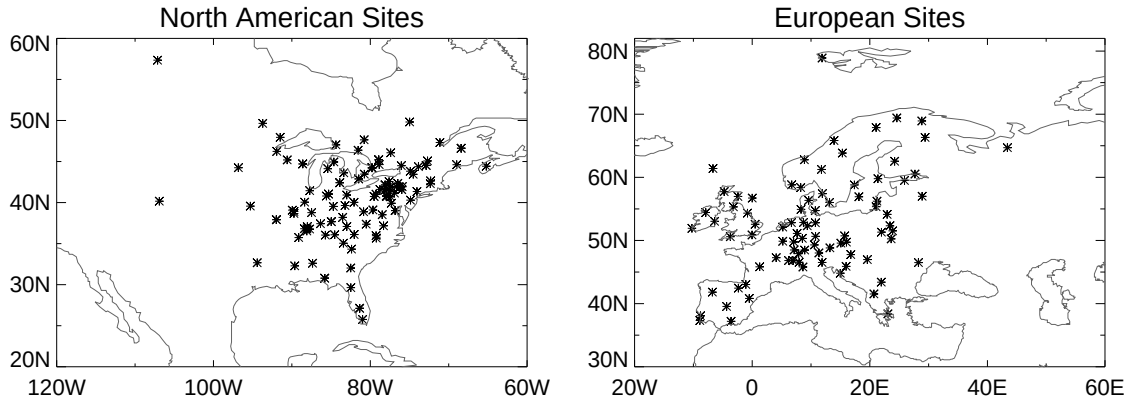
North American Sites
60N
50N
40N
30N
20N
120W
100W
80W
60W
European Sites
80N
70N
60N
50N
40N
30N
20W
0
20E
40E
60E

Figure 1

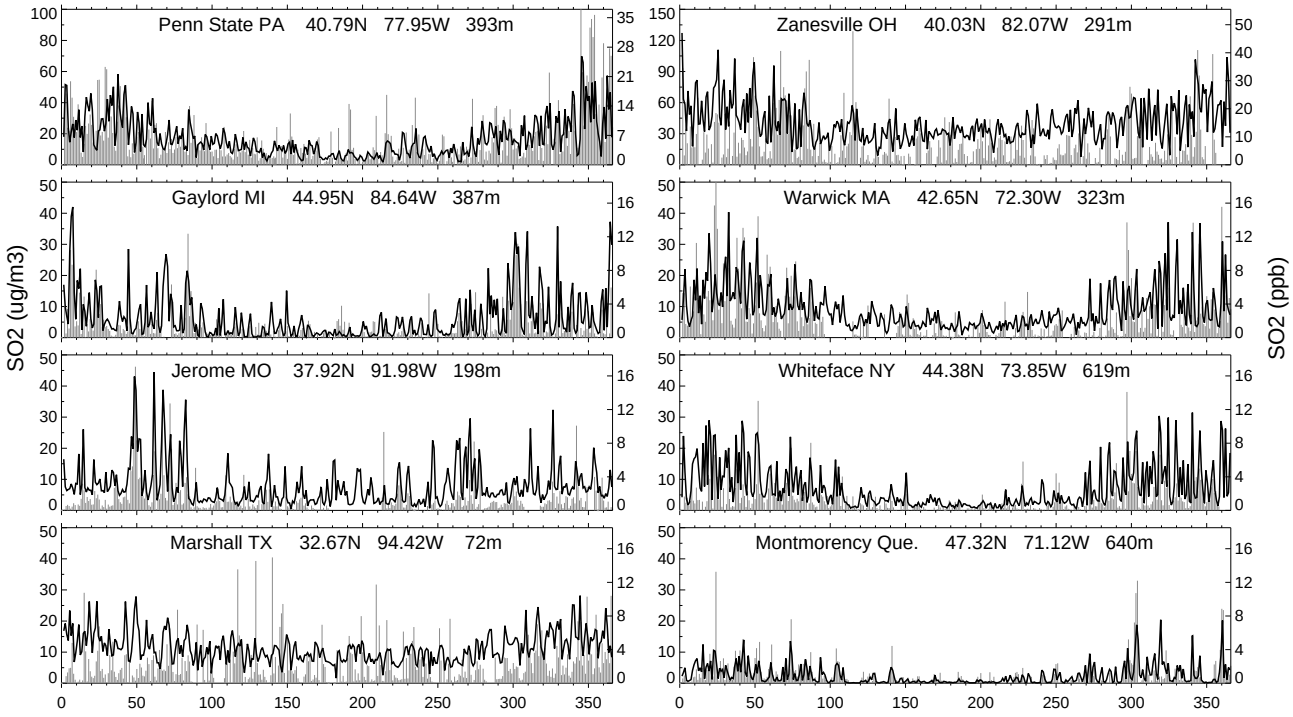

Figure 2a

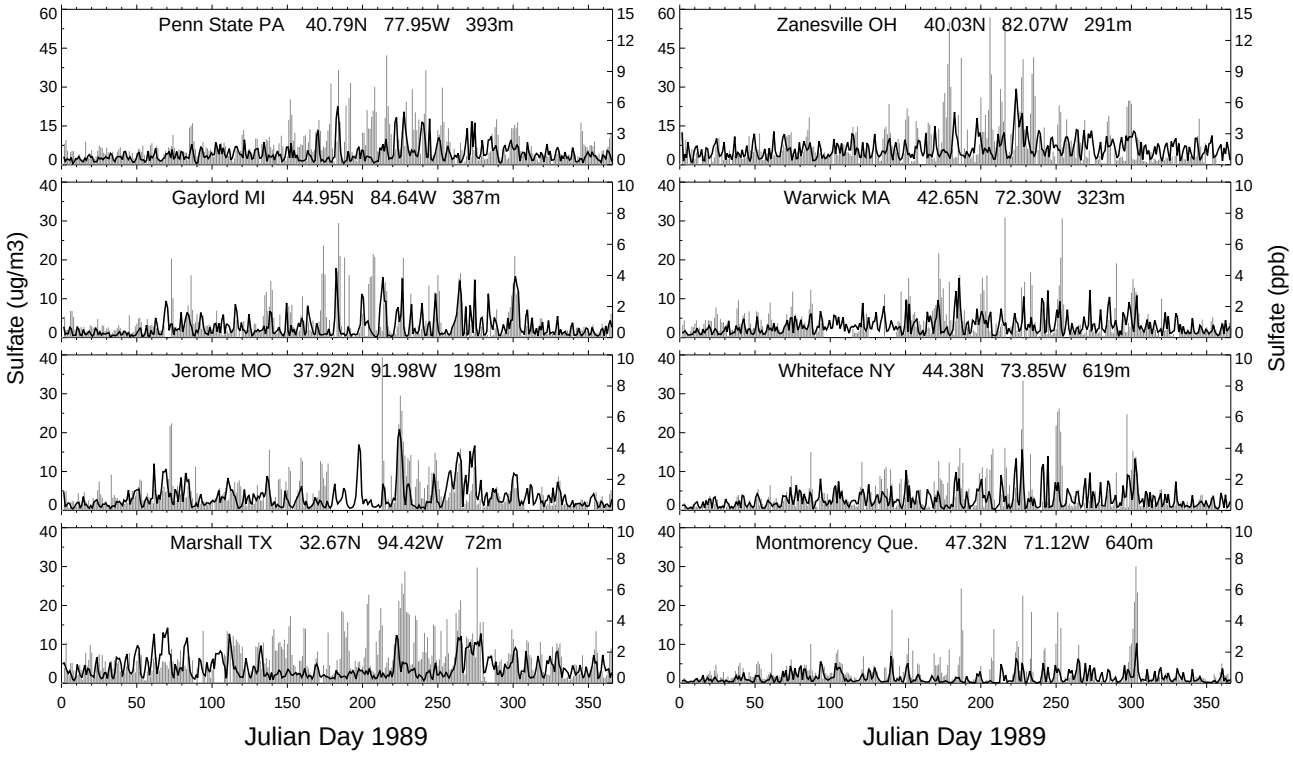

Figure 2b

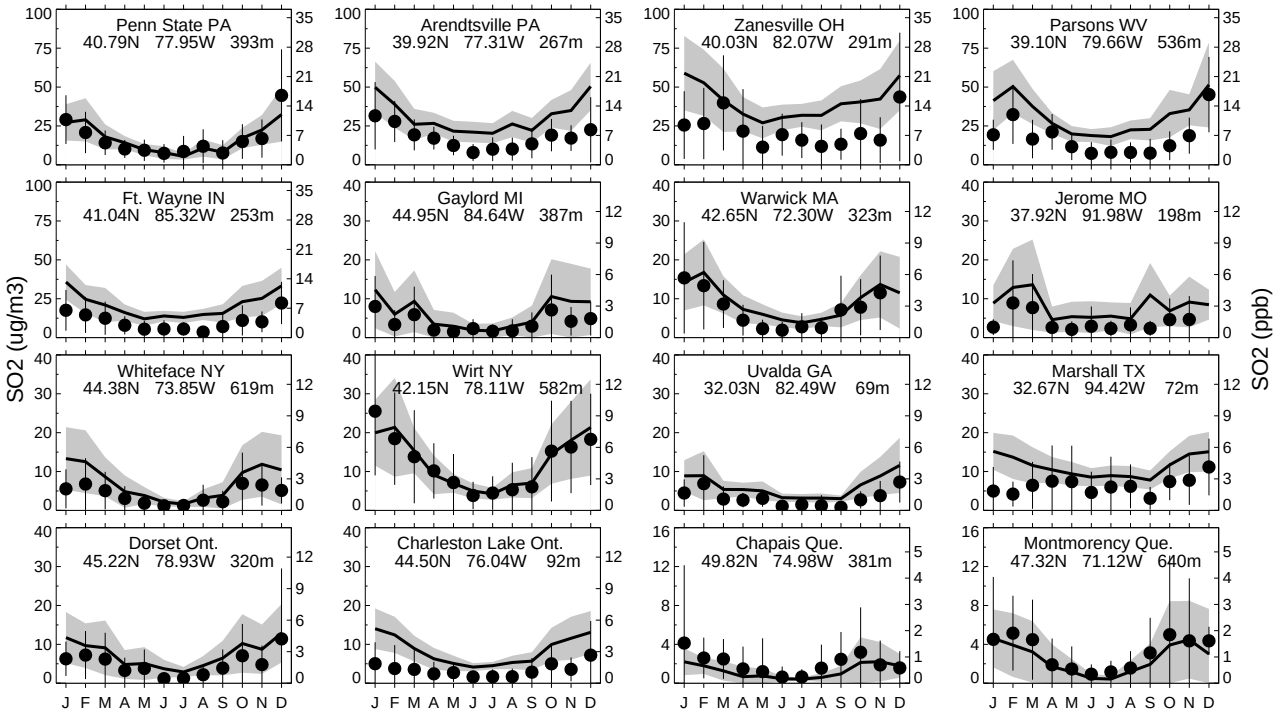

Figure 3a

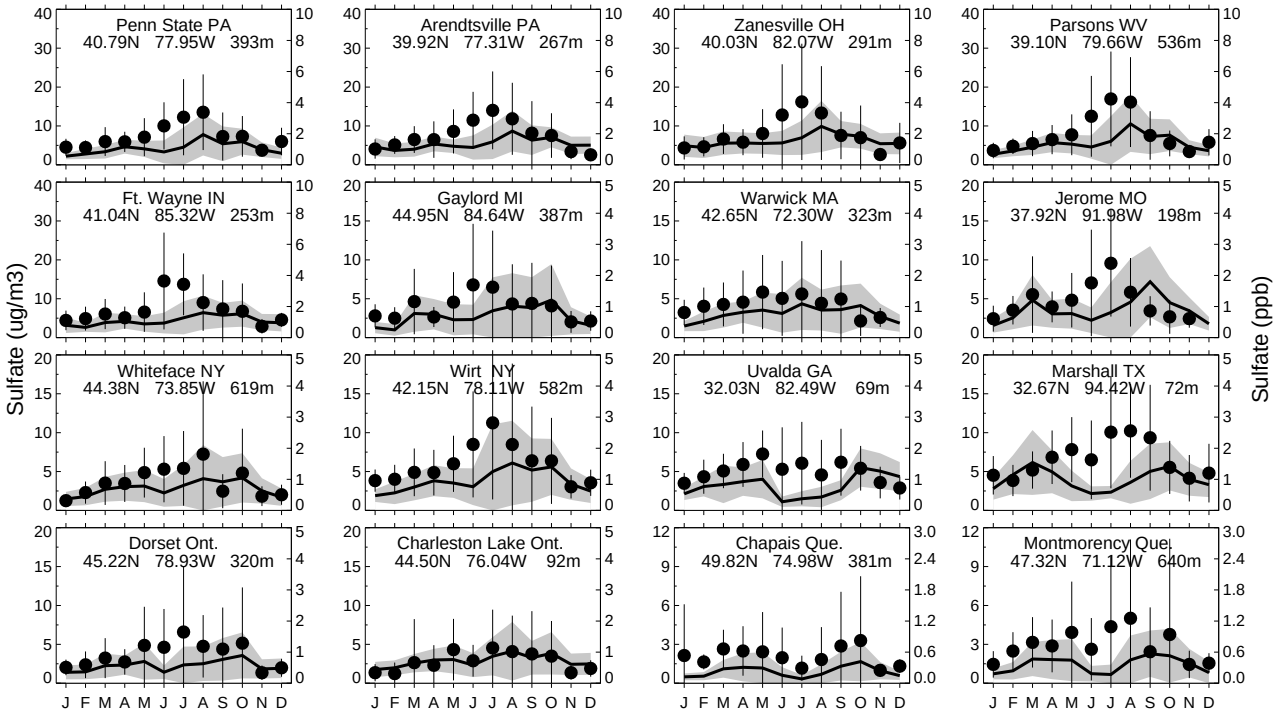

Figure 3b

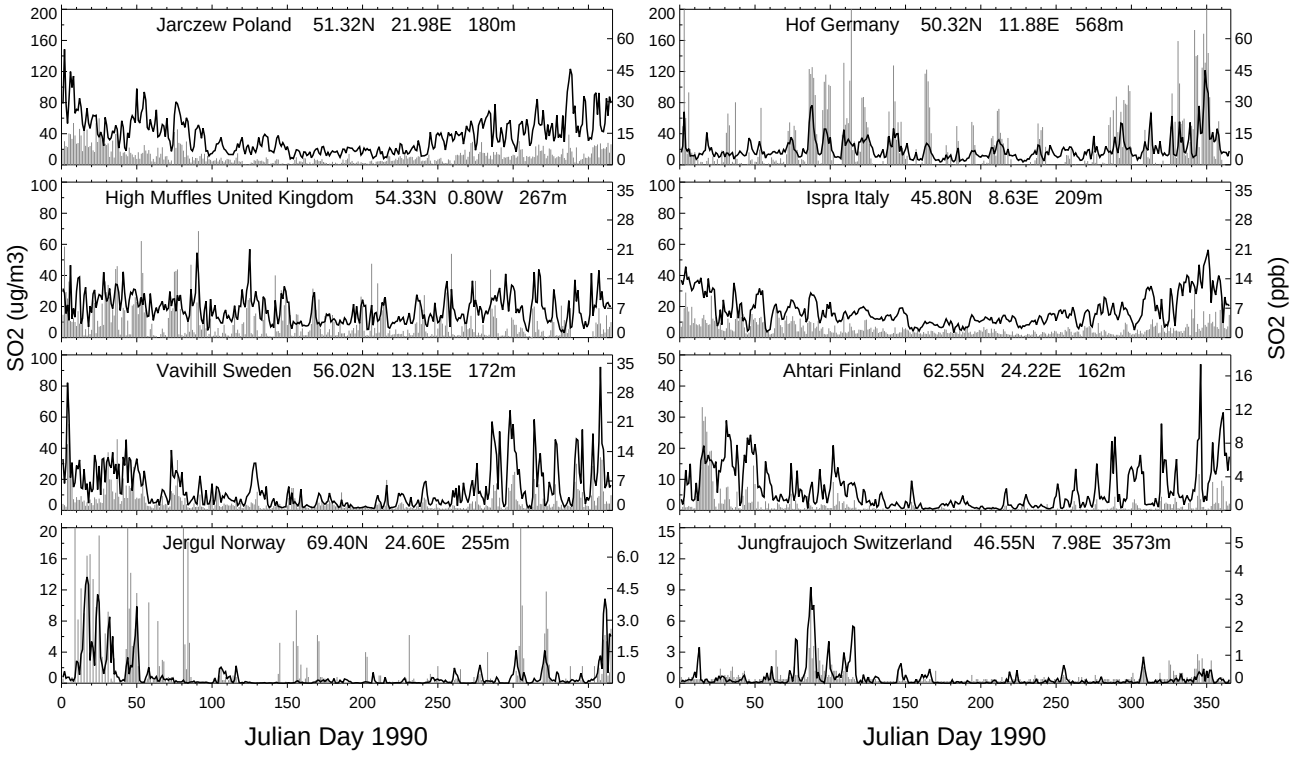

Figure 4a

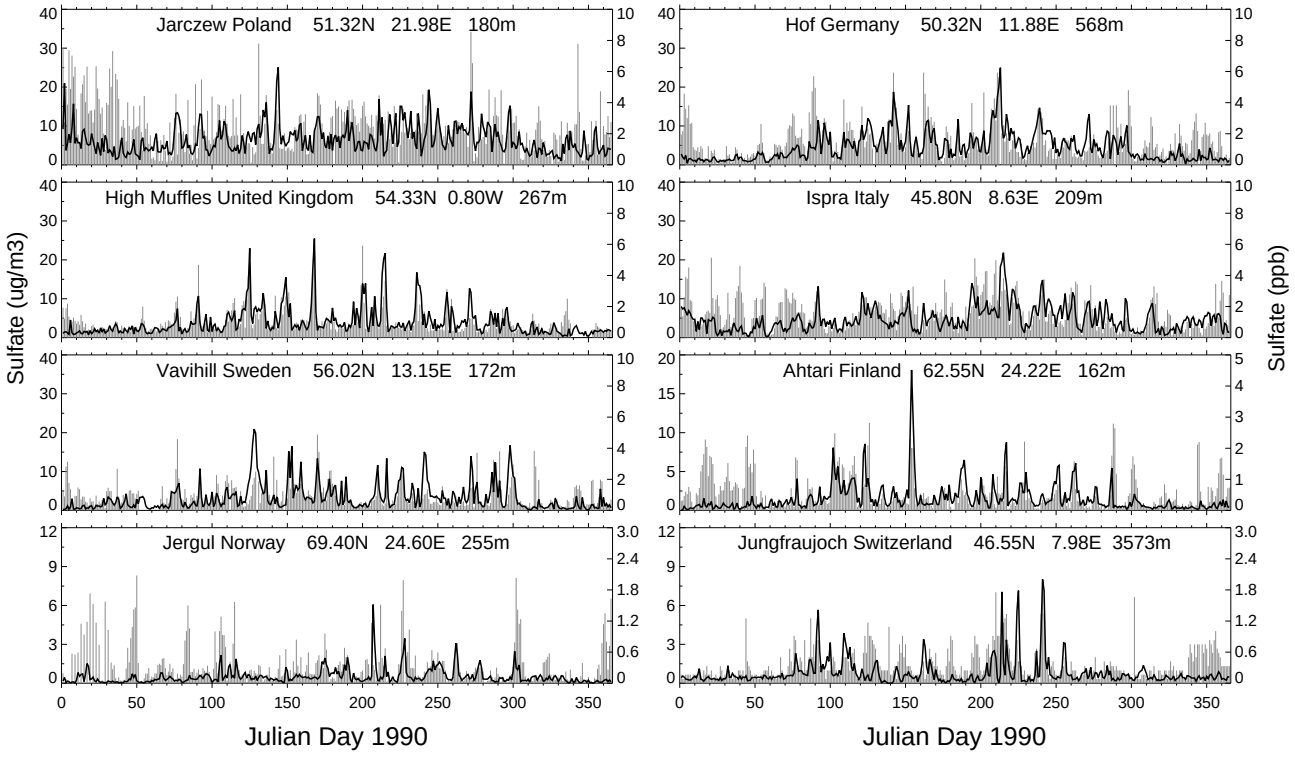

Figure 4b

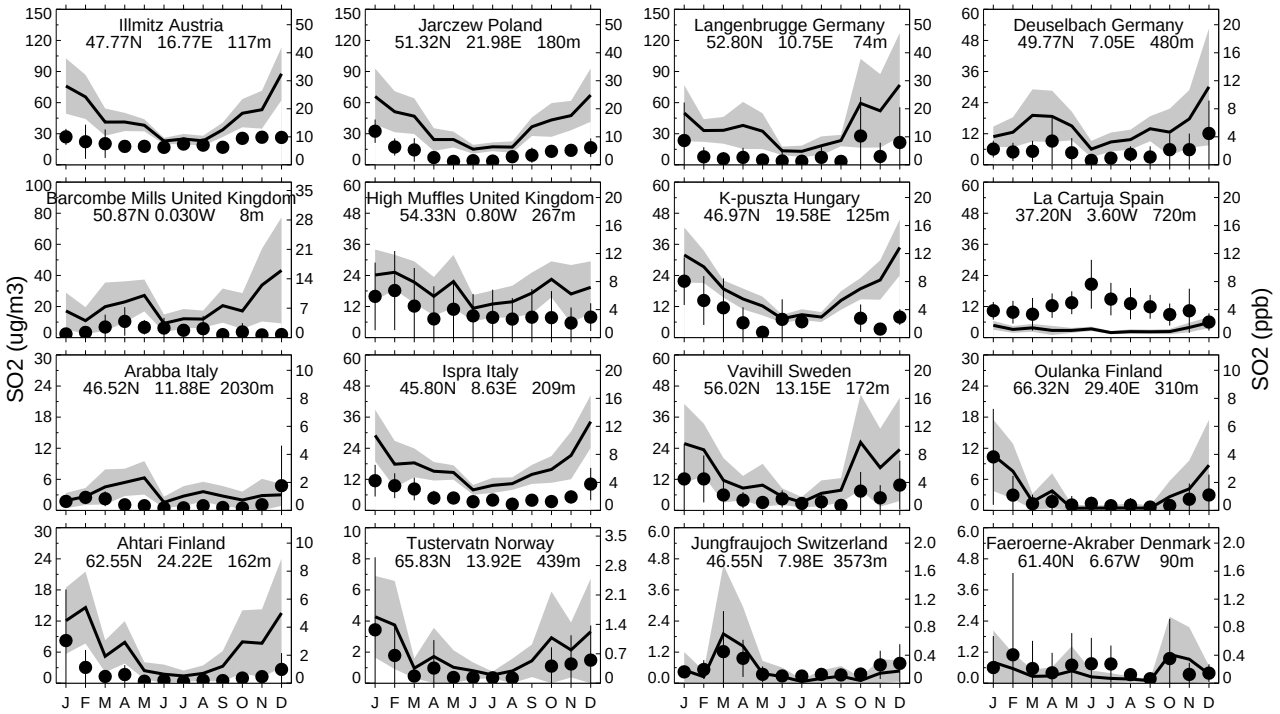

Figure 5a

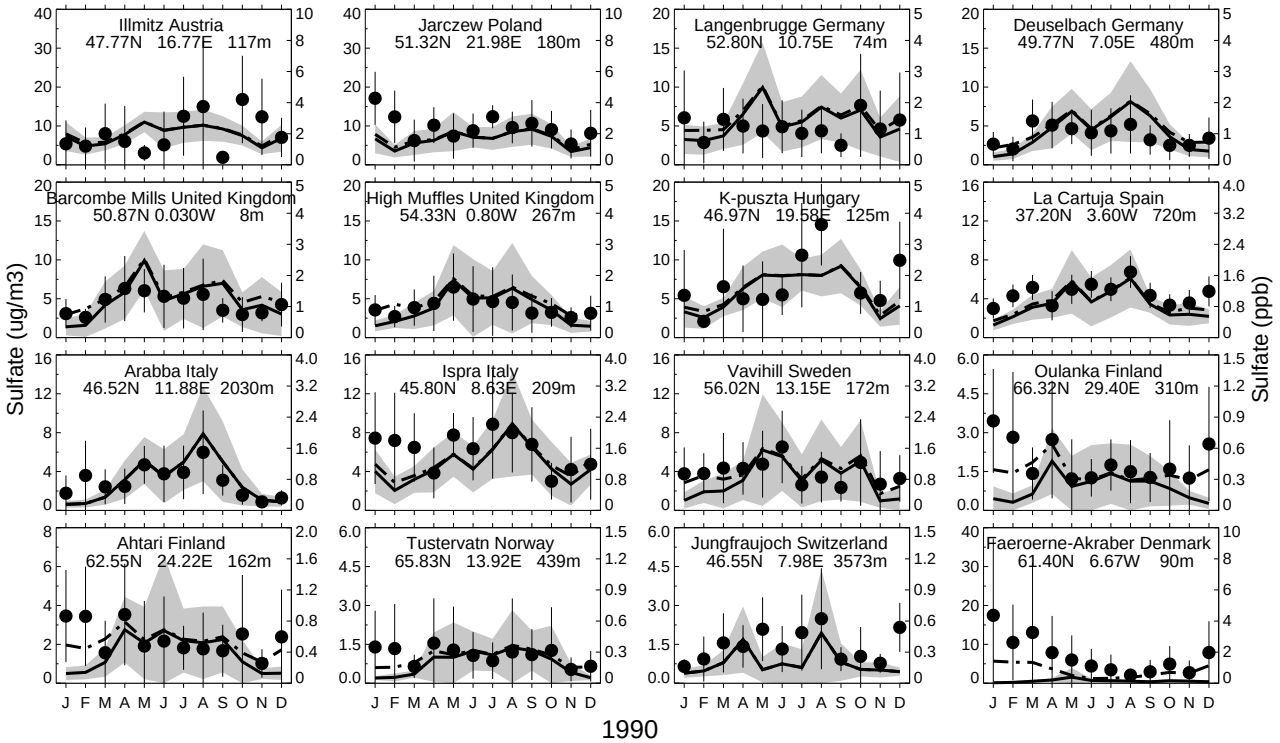

Figure 5b

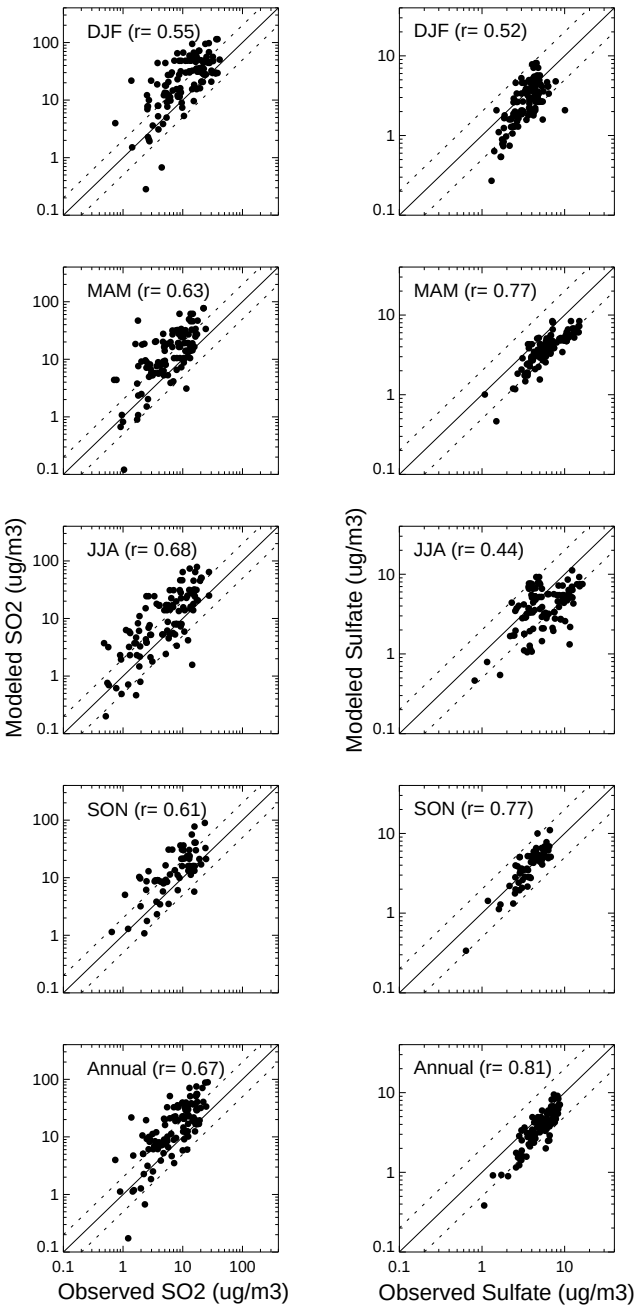
DJF (r= 0.55)
DJF (r= 0.52)
MAM (r= 0.63)
MAM (r= 0.77)
JJA (r= 0.68)
JJA (r= 0.44)
SON (r= 0.61)
SON (r= 0.77)
Annual (r= 0.67)
Annual (r= 0.81)
Modeled SO2 (ug/m3)
Modeled Sulfate (ug/m3)
Observed SO2 (ug/m3)
Observed Sulfate (ug/m3)
0.1
1
10
100

Figure 6

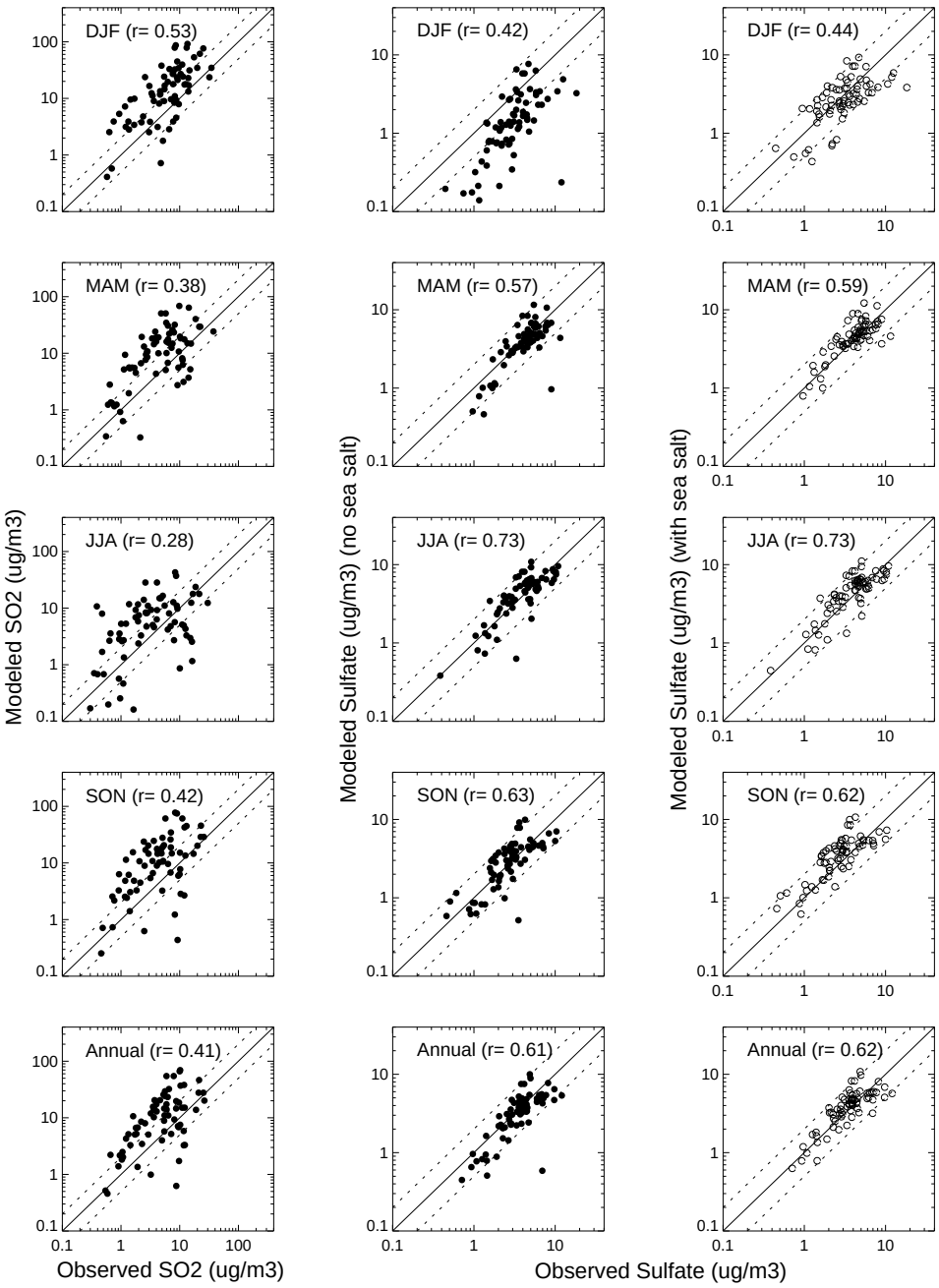
DJF (r= 0.53)
DJF (r= 0.42)
DJF (r= 0.44)
MAM (r= 0.38)
MAM (r= 0.57)
MAM (r= 0.59)
JJA (r= 0.28)
JJA (r= 0.73)
JJA (r= 0.73)
SON (r= 0.42)
SON (r= 0.63)
SON (r= 0.62)
Annual (r= 0.41)
Annual (r= 0.61)
Annual (r= 0.62)
Modeled SO2 (ug/m3)
Modeled Sulfate (ug/m3) (no sea salt)
Modeled Sulfate (ug/m3) (with sea salt)
Observed SO2 (ug/m3)
Observed Sulfate (ug/m3)

Figure 7

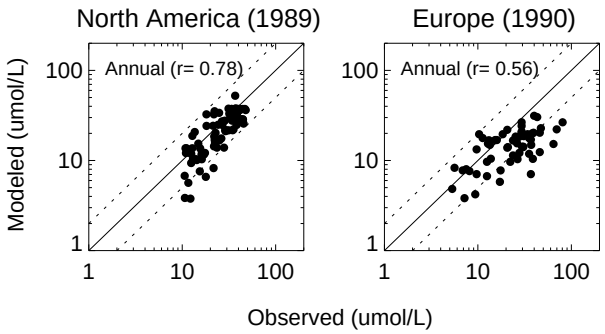
North America (1989)
Europe (1990)
Annual (r= 0.78)
Annual (r= 0.56)
Modeled (umol/L)
Observed (umol/L)
100
10
1
1
10
100

Figure 8

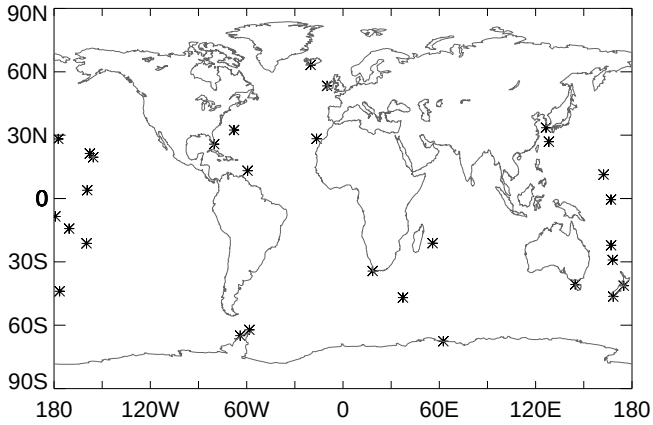

Figure 9

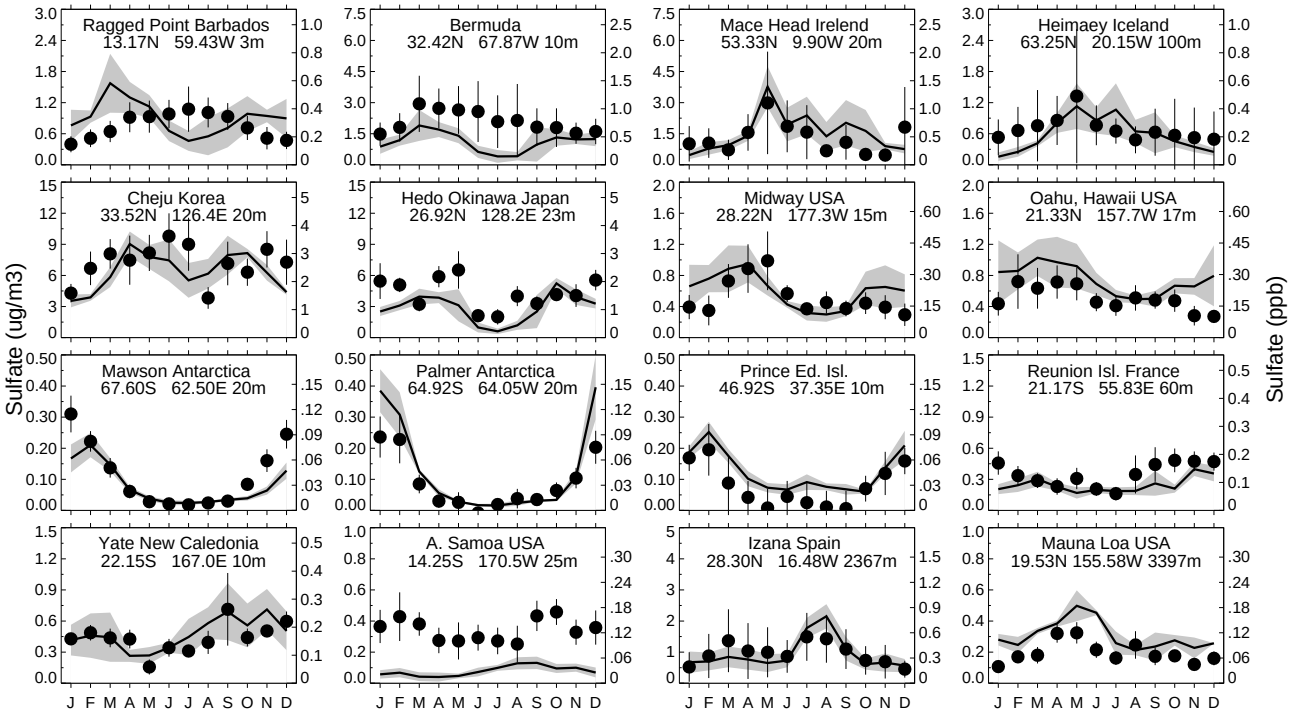

Figure 10a

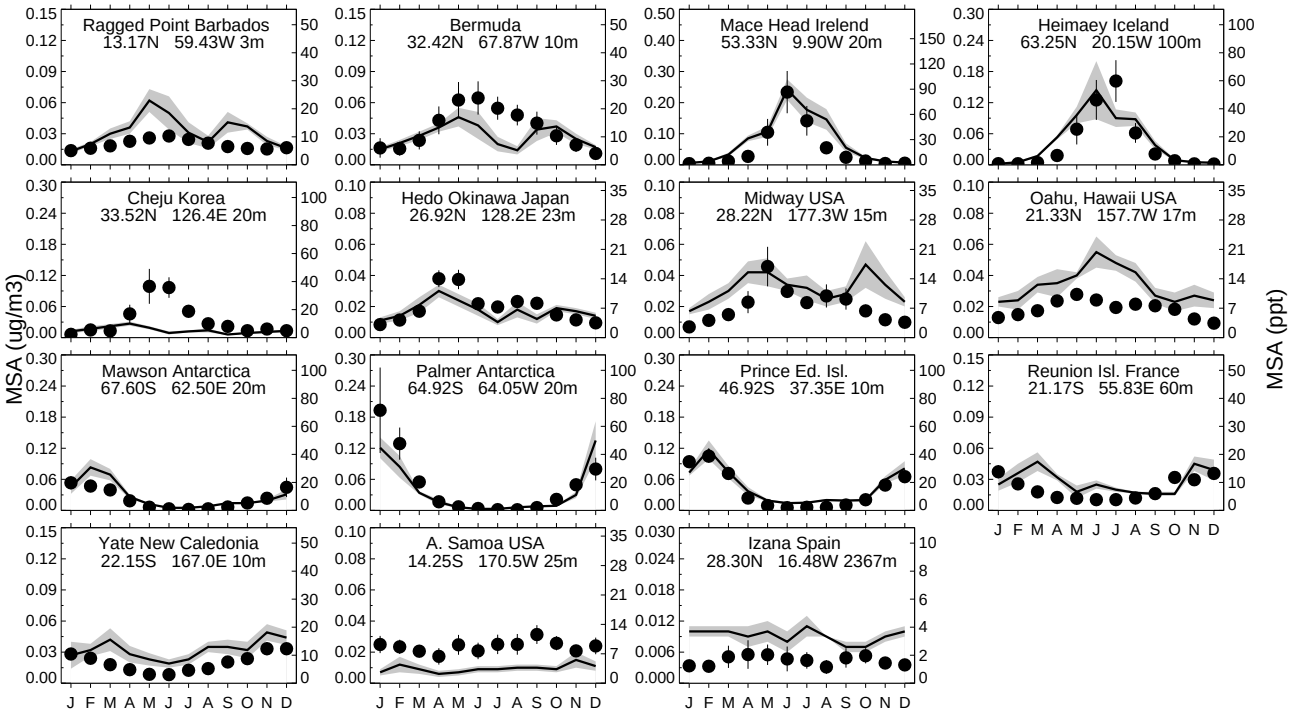

Figure 10b

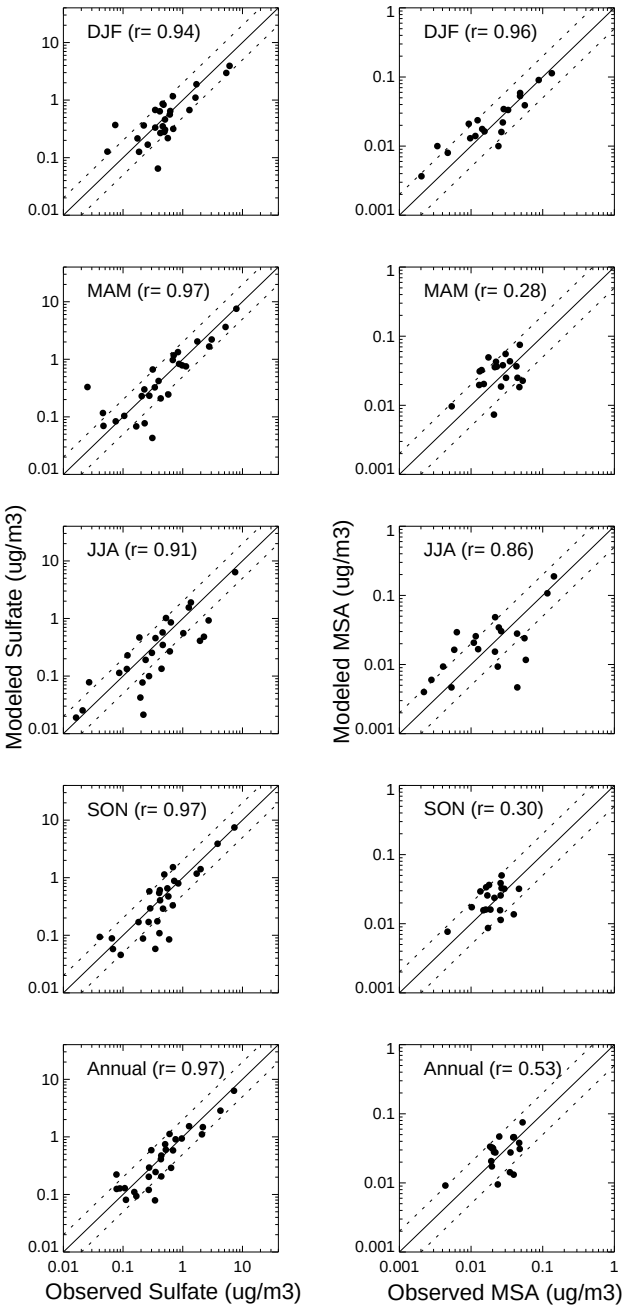
DJF (r= 0.94)
DJF (r= 0.96)
MAM (r= 0.97)
MAM (r= 0.28)
JJA (r= 0.91)
JJA (r= 0.86)
SON (r= 0.97)
SON (r= 0.30)
Annual (r= 0.97)
Annual (r= 0.53)
Modeled Sulfate (ug/m3)
Modeled MSA (ug/m3)
Observed Sulfate (ug/m3)
Observed MSA (ug/m3)

Figure 11

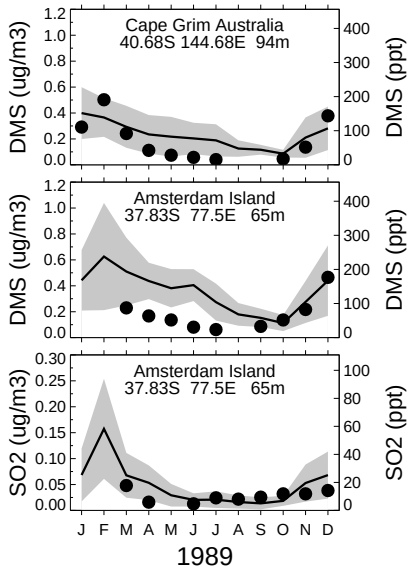
Cape Grim Australia
40.68S 144.68E 94m
DMS (ug/m3)
DMS (ppt)
Amsterdam Island
37.83S 77.5E 65m
DMS (ug/m3)
DMS (ppt)
Amsterdam Island
37.83S 77.5E 65m
SO2 (ug/m3)
SO2 (ppt)
J F M A M J J A S O N D
1989

Figure 12

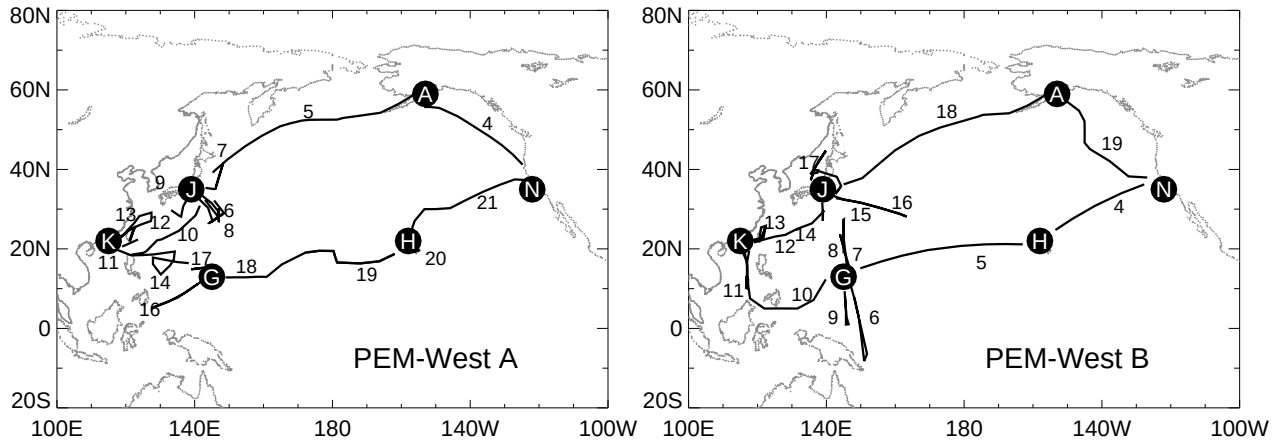
80N
60N
40N
20N
0
20S
100E
140E
180
140W
100W
A
N
J
K
G
H
PEM-West A
PEM-West B

Figure 13

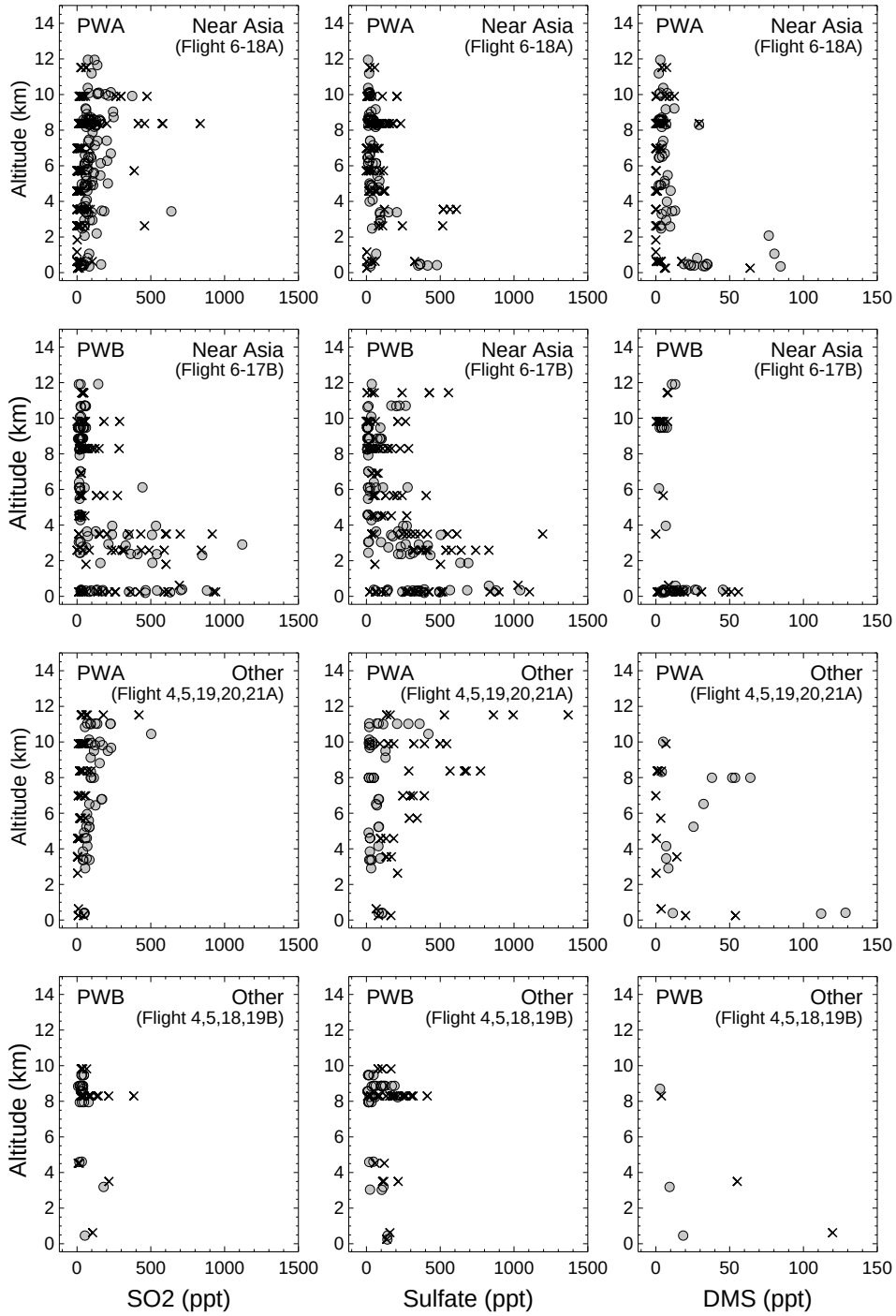
PWA
Near Asia
(Flight 6-18A)
PWB
Near Asia
(Flight 6-17B)
PWA
Other
(Flight 4,5,19,20,21A)
PWB
Other
(Flight 4,5,18,19B)
Altitude (km)
SO2 (ppt)
Sulfate (ppt)
DMS (ppt)

Figure 14

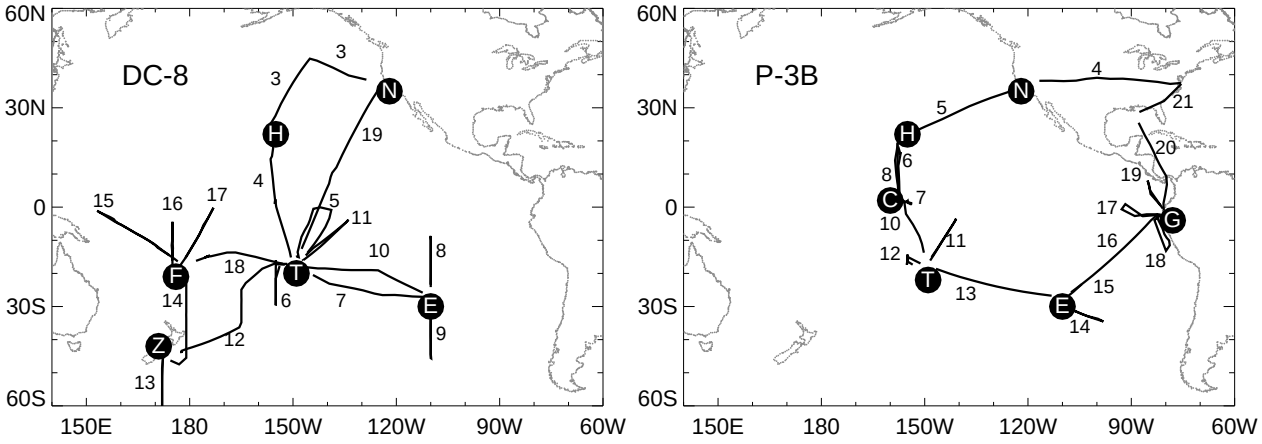

Figure 15

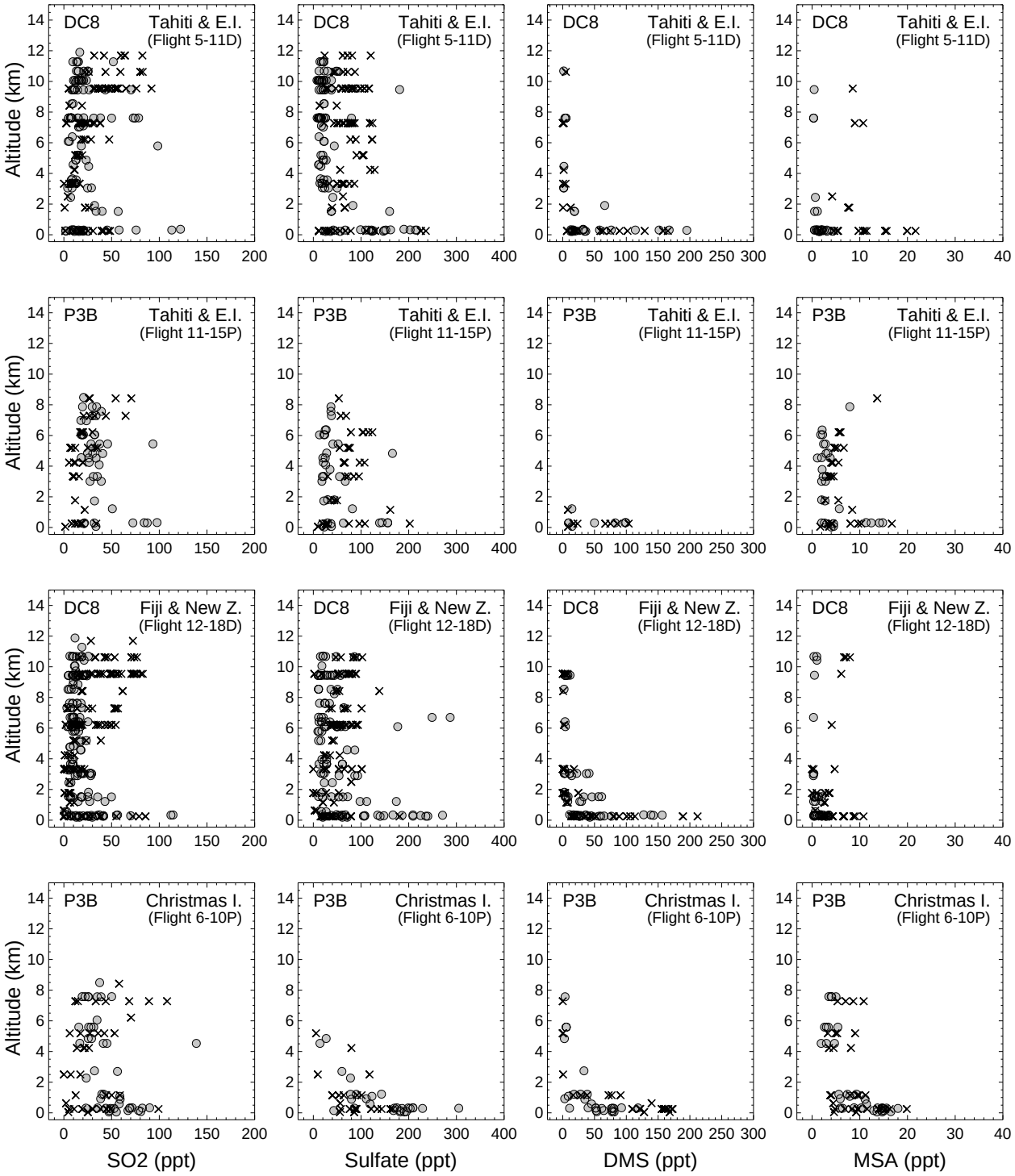
DC8 Tahiti & E.I. (Flight 5-11D)
P3B Tahiti & E.I. (Flight 11-15P)
DC8 Fiji & New Z. (Flight 12-18D)
P3B Christmas I. (Flight 6-10P)
Altitude (km)
SO2 (ppt)
Sulfate (ppt)
DMS (ppt)
MSA (ppt)

Figure 16

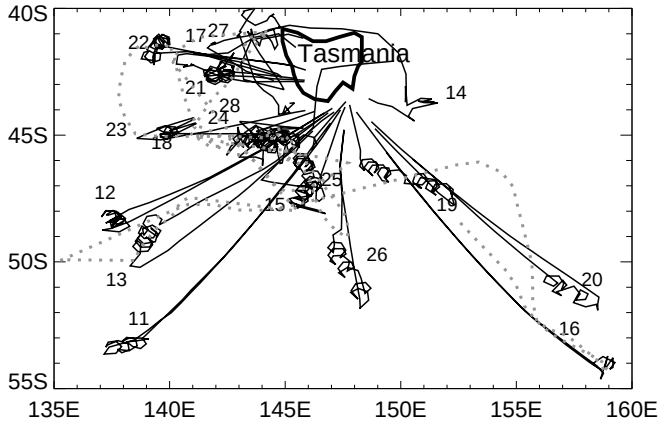
40S
45S
50S
55S
135E
140E
145E
150E
155E
160E
Tasmania
11
12
13
14
15
16
17
18
19
20
21
22
23
24
25
26
27
28

Figure 17

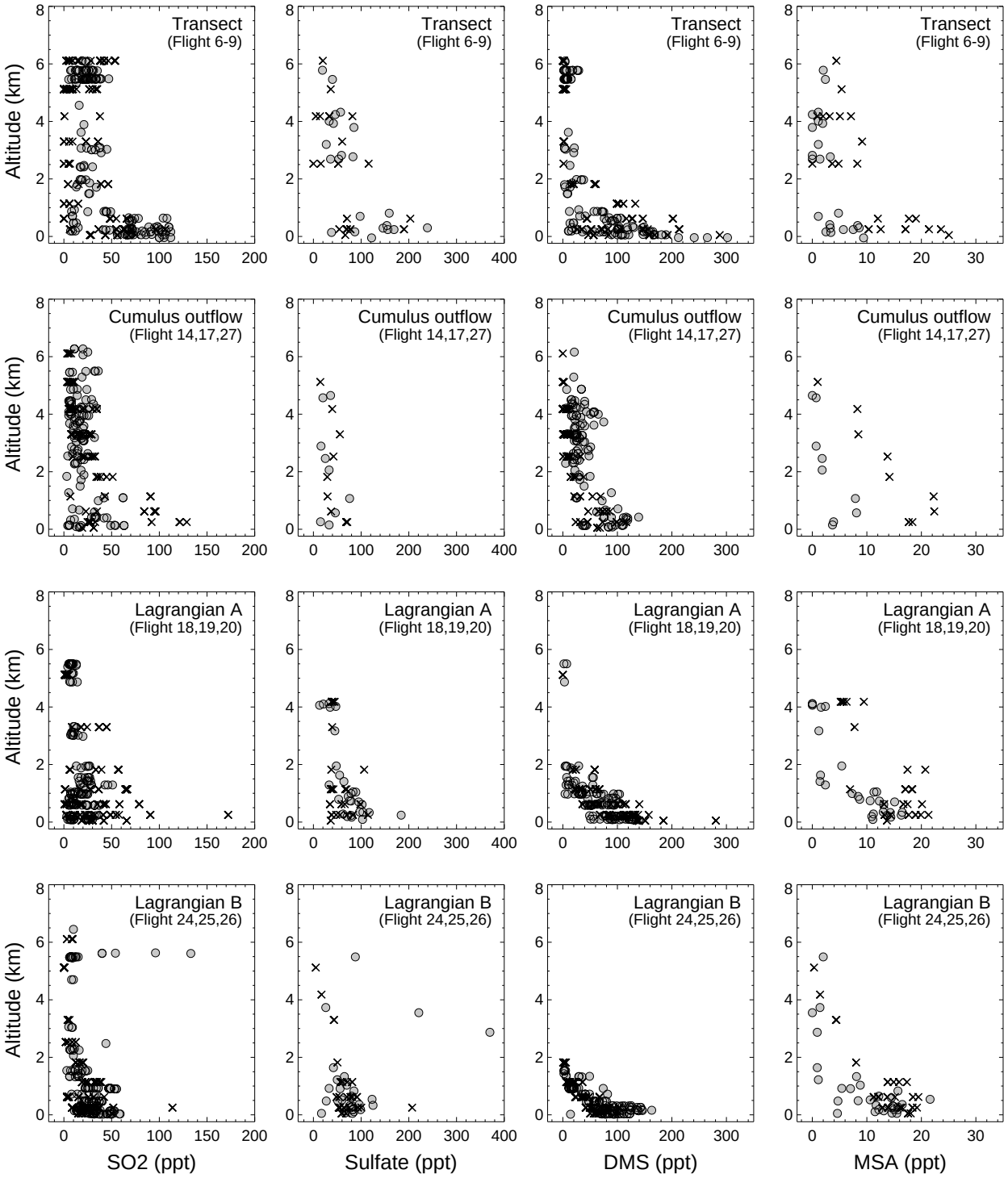
Transect
(Flight 6-9)
Cumulus outflow
(Flight 14,17,27)
Lagrangian A
(Flight 18,19,20)
Lagrangian B
(Flight 24,25,26)
Altitude (km)
SO2 (ppt)
Sulfate (ppt)
DMS (ppt)
MSA (ppt)

Figure 18

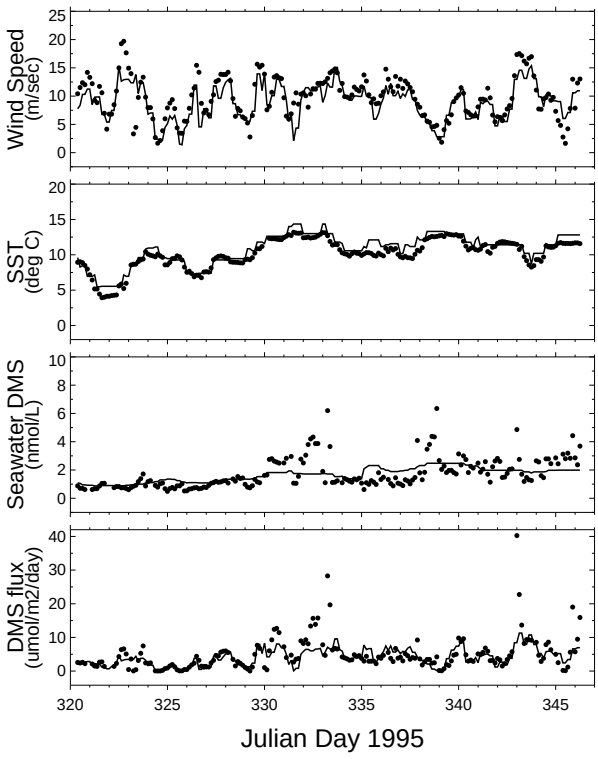
Wind Speed
(m/sec)
SST
(deg C)
Seawater DMS
(nmol/L)
DMS flux
(umol/m2/day)
Julian Day 1995

Figure 19

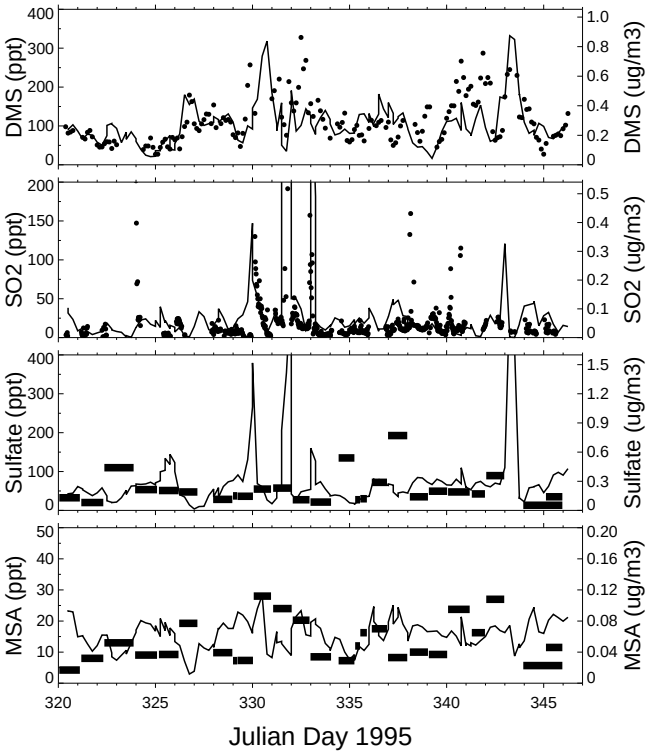
DMS (ppt)
DMS (ug/m3)
SO2 (ppt)
SO2 (ug/m3)
Sulfate (ppt)
Sulfate (ug/m3)
MSA (ppt)
MSA (ug/m3)
Julian Day 1995

Figure 20

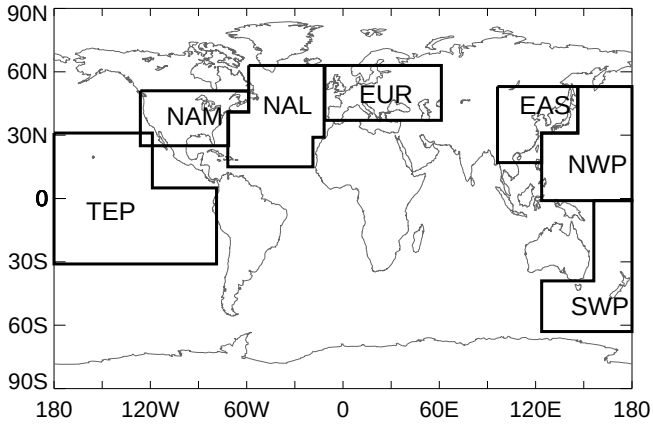
90N
60N
30N
0
30S
60S
90S
180
120W
60W
0
60E
120E
180
NAM
NAL
EUR
EAS
NWP
TEP
SWP

Figure 21